Dissertation

Theoretical Study on the Properties and Sensitivity of Organic Compounds with Characteristic Bonds

(特異な結合を有する有機化合物の性質と感応性に関する理論的研究)

Yusuke Kuroda

Hokkaido University
Graduate School of Chemical Sciences and Engineering
Quantum Chemistry Laboratory
（北海道大学大学院総合化学院 量子化学研究室）

2019

Contents

1 General Introduction

1.1 Characteristic Chemical Bond

A chemical bond is an interaction among two or more atoms in molecules, ions, crystals, and other stable species. When forces act to attract atoms to form an aggregation, atoms approach one another. Then, their nuclei and electrons interact and distribute themselves in space in such a way that the total energy is low to ensure a sufficient stability[1]. There are three kinds of typical strong chemical bonds. Covalent bonds are formed by overlapping orbitals of atoms, and ionic bonds are strongly connected with atoms by electrostatic interaction. Metal bonds mean a state in which the atoms are regularly arranged like crystals in metals, and electrons move freely between respective atoms[2].

I focus on covalent bonds in organic chemicals. Ordinary covalent bonds are formed by overlapping orbitals, which are derived from s and p orbitals, and electrons are shared among atoms connected by bonding. Two electrons are usually shared in a set of overlapping orbitals. In organic chemicals, a pair of s orbitals, p orbitals, or s orbital and p orbital form σ bond overlap. When π bonds be located at the same position as σ bonds, the π orbitals will form in the direction perpendicular to the axis including the single bond formed by the σ orbitals. Generally, the chemical bonds in the organic chemicals consist of combinations of σ bonds and π bonds. The atoms of organic chemicals which do not contain metal atoms keep the octet rule, that is, the state where 8 electrons are located in the periphery of each atom[3, 4].

I define the characteristic bonds among covalent bonds in organic compounds as those having a different bonding model from that of an ordinary covalent bond. It includes a

bond with a small overlap of orbitals. The overlap of orbitals has become smaller due to some actions, and the bonds are stretched. Such characteristic bonds are weaker compared to average chemical bonds. Thus, they are involved with some reactions, or show a change in the physical properties of the substance itself.

I do not refer to the bonds in the conjugated systems like 1,3-butadiene as characteristic bonds, which have alternate combinations of multiple bonds including π bonds and single bonds (σ bonds). Via the neighboring σ bond of a single bond, the p orbitals of each atom which constitute multiple bonds on both sides interact with each other[5]. In this case, the delocalization of electrons is confirmed by conjugation, the extension of the double bond and the contraction of the single bond are confirmed.

The organic compound having such a characteristic bond is subjected to external stimuli such as heat, light, and electron donation whereby its characteristic bond is eliminated, and causes the conversion of the molecule or the change in physical properties. I define a compound with such properties as a stimuli-responsive compound.

However, compounds having such characteristic bonds with a simple structural design are unstable and might compete with other unnecessary reactions or decompositions. The characteristic bonds are often long, and weak on the definition in this dissertation. Therefore, it is difficult to use such compounds for further use as materials, and the use of rigid skeletons is required to stabilize themselves and show the desired change. Nevertheless, it has become possible recently to precisely synthesize such a compound having a complicated structure, because there have been few methods to synthesize them in high yields. The number of researches conducted by theoretical calculations was still small, and there are room to research in this field.

I chose the two kinds of characteristic chemical bonds, a 3-center-4-electron bond and an ultralong covalent bond. For such bonds, there are experimental researches which are involved with stimuli-responsive properties. In addition, there are chances to apply the theoretical performance and to yield the further developments of “responsive compounds.”

1.2 Three-Center Four-Electron Bond

A 3-center 4-electron bond (3c-4e bond) is a bonding model in which there are four electrons connecting three atoms. Such bonds are confirmed in typical element compounds where nine or more electrons are present. Such compound is called hypervalent compounds[6]. When and ligands located around the atom with more than 8 electrons, they form a structure like a complex.

In the 3c-4e bond model, there are three kinds of molecular orbitals, a bonding orbital, a nonbonding orbital, and an antibonding orbital. Also, Figure 1 shows the bonding orbital of the 3c-4e bond (triiodide, I_3^-). The bonding and antibonding orbitals are of odd symmetry, and nonbonding orbitals are of even symmetry[7]. The 3c-4e bond are formed by the σ orbitals, or π orbitals. The central atom offers a pair of electrons (two electrons) to the orbital, and each ligand offers one electron. The four electrons fill the bonding and nonbonding orbitals, like Figure 1[8].

There are organic and inorganic typical element compounds which have a 3c-4e bond. For example, the organic compounds with a 3c-4e bond are hypervalent typical element organic compounds such as pentaphenoxyphosphorane ($(C_6H_5O)_5P$), and hypervalent carbon compounds[9-20]. The inorganic compounds examples are ozone (O_3), and I_3^-. I_3^- maintains bonds to share 4 electrons by two bonds of iodine atoms, and such a connection is developed linearly. The central atom violates the octet rule formally. In addition, recently, there has been a report investigating the influences of the bond property by using the electron donating or the withdrawing property in the surrounding periphery of the 3c-4e bond[21]. In the case of pentaphenoxyphosphorane, it is a hypervalent compound having a structure like the above-mentioned complex, and five phenoxy groups are positioned around the phosphorus atom[9]. The bond length of 3c-4e bond is longer than

that of general covalent bond (also described in Chapter 2). In addition, The I–I bond of I_3^- is longer than the that of I_2, a diatomic molecule.

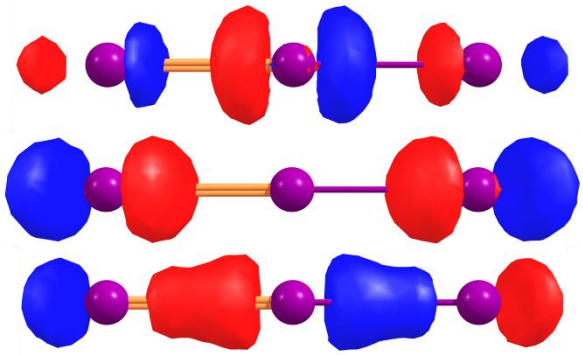

Figure 1. The orbitals of 3c-4e bond of I_3^- (Top: Anti-bonding orbital, Center: Nonbonding orbital, Bottom: Bonding orbital).

1.3 Characteristic Structure of Covalent Bond Length

The bond length, bond angle, and distortion angle (I also call it dihedral angle or twist angle) are three elements of internal coordinates that determine the structure of the molecule. Such internal coordinates have been clarified by experimental methods such as X-ray crystal structure analysis and electron beam diffraction. The interatomic distance when two atoms are connected by a covalent bond is often within a certain range without depending on the type of molecule or crystal.

On the other hand, some of the compounds also have internal coordinates that do not fit within this range of the degree of internal coordinates. Considering a covalent bond as an example, covalent bonds are formed by overlapping orbitals of atoms. When the overlapping of the orbitals becomes small, the strength of a bond weakens, and the bond length expands accordingly. If the overlap of the orbitals becomes larger, the opposite phenomenon occurs. The phenomenon in which the strength of the bond changes due to the large/small overlap of these orbitals is often seen with a single bond, and in multiple bonds it is not seen except for conjugation.

The extension causes due to the steric repulsion or the ring structure that the overlap of the orbitals forming the bond becomes smaller. Researchers believe that the existence of bulky substituents and rigid frameworks in the periphery limits the range of movement of skeletons around the bond length. Therefore, there have been reports that compounds having long covalent bonds can be obtained and the surroundings are cyclic structures, substituents containing aromatic rings. This phenomenon can be confirmed although the atoms forming the bond are not homogeneous. In the case of multiple coupling, there are not many cases where it is possible to confirm the extension of the coupling due to shortening of the overlapping region of orbitals due to steric repulsion. For a long time, a

lot of researchers have synthesized compounds with long covalent bond (mainly C–C bond), and they have done theoretical analyses[22-25]. In addition, since the bond length of the 3c-4e bond described in the previous section is longer than that of the general covalent bond, the compound having an internal coordinate (bond length) having such unusual parameter It is also possible to include it. In this paper I focus on covalent bond length.

1.4 DFT Calculation

When finding the electronic state of a substance by quantum chemical calculation, I need to solve the Schrödinger equation.

$$H\Psi = E\Psi \tag{1.1}$$

H in the above equation is Hamiltonian, E is energy, and Ψ is a wave function. Hamiltonian H is required as follows[26].

$$H = -\frac{\hbar^2}{2m}\sum_{i=1}^{N}\nabla_i^2 + \sum_{i=1}^{N}V(\mathbf{r}_i) + \sum_{i=1}^{N}\sum U(\boldsymbol{r}_i, \boldsymbol{r}_j) \tag{1.2}$$

It is very difficult to solve the Schrödinger equation exactly, except for a very simple case like H_2^+. Therefore, it is common to solve using approximation.

One of the methods to approximate this Schrödinger equation is density functional theory calculation and DFT calculation. Solve the Kohn-Sham equation

$$[-\frac{\hbar^2}{2m}\nabla^2 + V(\mathbf{r}) + V_H(\mathbf{r}) + V_{XC}(\mathbf{r})]\psi_i(\mathbf{r}) = \varepsilon_i\psi_i(\mathbf{r}) \tag{1.3}$$

and approximate the electronic state. What is different from the Schrödinger equation is that the Hamiltonian H does not include summations comparing to Schrödinger equation. This is because the solution obtained by the Schrödinger equation depends on three spatial variables[26].

In this study, I carried out the calculations for the hypervalent organic compounds

synthesized in the experiment or the organic compounds having the bond showing a larger value than the general bond length. Although the organic molecule to be taken up here is a low molecule, there are cases in which the crystal structure is taken into consideration. Therefore, I decided to apply DFT calculation for calculation efficiency and agreement with experimental data.

1.5 Dispersion energy

Fritz London supposed the concept, London force when thinking the attraction of the approach between noble gas atoms[27]. London force is that which causes when atoms or moieties of molecule approach to each other, and it is treated as a kind of Van der Waals forces. In general, the London dispersion force is inversely proportional to r^6. r means length between atoms.

The stretch and contraction of the covalent bond occur because of the molecule structure. The steric repulsion of the bulky substituents is one of the most possible reasons. In addition, some bulky substituents and skeletons have rigid π skeletons and the intramolecular interactions are expected because of the location of the π skeletons. Such interactions can be treated as a kind of London force, long-range interaction. Therefore, I need to consider the dispersion, London force on the theoretical researches in the space where the π-π intramolecular interaction causes.

1.6 General Purpose of This Dissertation

Characteristic bonds refer to a bond having properties different from general single bonds or multiple bonds. Compounds with such bonds cause changes in physical properties and conversions to species which have high energies due to external stimuli. Theoretically analyzing the characteristic bond of organic compounds and understanding the properties at the electronic level is quite important to connection with the development of new reactions and physical properties. The purpose of this research is to clarify the electronic properties of the characteristic bond and to examine the capacity of "stimuli-responsive" compounds. In this research, there are two kinds of characteristic chemical bonds as targets, 3-center-4-electron bond and "ultralong" covalent bond. The compounds having such bonds have chemical species which show changes in physical properties involving the bonds, and changes to different chemical species against external stimuli. There is an expectation about calculation as a means when newly discovering materials that respond to external stimuli and materials that can be used as intermediates that produce other products efficiently. Ultimately, I aim at extracting elements related to changes in physical properties and the nature of bonds, and then clarifying the relationship between the two from the theoretical viewpoint.

1.7 Overview

This paper consists of the following five chapters.

First, Chapter 1 outlines this theme. I will explain how characteristic bonds are defined in this research and the parts that form the concept of the anomalous bonds of compounds dealt with in later chapters.

In chapter 2, I describe the reactions caused by hypervalent compounds with three centers and four electron bonds. In this research, I explain the theoretical analysis on chemical reactions caused by typical element compounds, especially hypervalent antimony (Sb) compounds.

In Chapter 3 and Chapter 4, I investigated C–C carbon single bonds greatly elongated by the surrounding steric structure. In chapter 3, I explore the reason why the "ultra-long" C–C single bond has been extended by theoretical calculation. Chapter 4 clarifies how the ultralong C–C single bond, synthesized in recently, will occur interesting phenomena using theoretical calculations.

In chapter 5 I describe general conclusions which derive from the results to summarize these researches in Chapter 2-4.

1.8 References

1. a) “Chemical bonding,” in Encyclopædia Britannica, Encyclopædia Britannica, inc., Chicago, 15th edn., **2010**; b) L. Pauling, The Nature of the Chemical Bond and the Structure of Molecules and Crystal: An Introduction to Modern Structural Chemistry, Cornell University Press, Ithaca, NY, 3rd edn., **1960**.
2. H. A. Lorentz, The Theory of Electrons, Teubner, Leipzig, **1916**.
3. G. N. Lewis, *J. Am. Chem. Soc.* **1916**, *38*, 762.
4. I. Langmuir, *J. Am. Chem. Soc.* **1919**, *41*, 868.
5. P. Muller, *Pure & Appl. Chem.* **1994**, *66*, 1077.
6. J. I. Musher, *Angew. Chem. Int. Ed.* **1969**, *8*, 54.
7. D. E. Woon, T. H. Dunning Jr., in The Chemical Bond 2, ed. by G. Frenking, S. Shaik, Wiley, Weinheim, **2014**, pp. 49-70.
8. Y.-S. Cheung, C.-Y. Ng, S.-W. Chiu, W.-K. Li, *J. Mol. Struct. (Theochem)* **2003**, *623*, 1.
9. F. Ramirez, A. J. Bigler, C. P. Smith, *J. Am. Chem. Soc.* **1968**, *90*, 3507.
10. R. Breslow, S. Garrat, L. Kaplan, D. La Follete, *J. Am. Chem. Soc.***1968**, *90*, 4051.
11. R. Breslow, L. Kaplan, D. La Follete, *J. Am. Chem. Soc.* **1968**, *90*, 4056.
12. T. R. Forbus Jr., J. C. Martin, *J. Am. Chem. Soc.* **1979**, *101*, 5057.
13. C. Martin, *Science*, **1983**, *221*, 509.
14. M. Hojo, T. Ichi, K. Shibato, *J. Org. Chem.* **1985**, *50*, 1478.
15. a) T. R. Forbus Jr., J. C. Martin, *Heteroat. Chem.* **1993**, *4*, 113; b) T. R. Forbus Jr., J. C. Martin, *Heteroat. Chem.* **1993**, *4*, 129; c) T. R. Forbus Jr., J. C. Martin, *Heteroat. Chem.* **1993**, *4*, 137.

16. K.-y. Akiba, M. Yamashita, Y. Yamamoto, S. Nagase, *J. Am. Chem. Soc.* **1999**, *121*, 10644.
17. K.-y. Akiba, Y. Moriyama, M. Mizozoe, H. Inohara, T. Nishii, Y. Yamamoto, M. Minoura, D. Hashizume, F. Iwasaki, N. Takagi, K. Ishimura, S. Nagase, *J. Am. Chem. Soc.* **2005**, *127*, 5893.
18. T. Yamaguchi, Y. Yamamoto, D. Kinoshita, K.-y. Akiba, Y. Zhang, C. A. Reed, D. Hashizume, F. Iwasaki, *J. Am. Chem. Soc.* **2008**, *130*, 6894.
19. N. Kano, H. Miyake, K. Sasaki, T. Kawashima, N. Mizorogi, S. Nagase, *Nat. Chem.* **2010**, *2*, 112.
20. a) D. H. R. Barton, S. A. Glover, S. V. J. Ley, *J. Chem. Soc., Chem. Commun.* **1977**, 266; b) S. A. Glover, *J. Chem. Soc., Perkin Trans. 1* **1980**, 1338.
21. A.-C. C. Carlsson, K. Mehmeti, M. Uhrbom, A. Karim, M. Bedin, R. Puttreddy, R. Kleinmaier, A. A. Neverov, B. Nekoueishahraki, J. Gräfestein, K. Rissanen, M. Erdélyi, *J. Am. Chem.* Soc. **2016**, *138*, 9853.
22. F. Toda, K. Tanaka, I. Sano, T. Isozaki, *Angew. Chem. Int. Ed. Engl.* **1994**, *33*, 1757.
23. G. Dyker, J. Körning, P. Bubenitschek, P. G. Jones, *Liebigs ann./Recueil* **1997**, 203.
24. a) T. Suzuki, J. Nishida, T. Tsuji, *Chem. Commun.* **1998**, 2199; b) T. Suzuki, J. Nishida, T. Tsuji, *Angew. Chem. Int. Ed. Engl.* **1997**, *36*, 1329.
25. G. Gunbas, N. Hafezi, W. L. Sheppard, M. M. Olmstead, I. V. Stoyanova, F. S. Tham, M. P. Meyer, M. Mascal, *Nat. Chem.* **2012**, *4*, 1018.
26. D. S. Sholl, J. A. Steckel, DENSITY FUNCTIONAL THEORY A practical introduction, Wiley, Hoboken, **2009**.
27. F. London, *Trans. Faraday Soc.* **1937**, *33*, 8.

2 Ligand Coupling Reaction of Hypervalent Antimony Compounds

2.1 Pentaarylantimony Compounds

A pentaarylantimony compound is considered as a typical hypervalent compound characterized by the three-center four-electron (3c-4e) bond. They show characteristic properties and reactivities arising from the 3c-4e bond[1], for example, trigonalbipyramidal structure (the crystal structure of Ph_5Sb is a well-known exception that shows the square pyramidal shape)[2], apicophilicity (the character that electron withdrawing ligands tend to occupy apical positions)[3], Berry pseudo-rotation[4], ligand exchange reaction (LER), and ligand coupling reaction (LCR). LCR of Ph_5Sb to quantitatively afford biphenyl and triphenylantimony was reported by Wolf and co-workers[5]. They also carefully observed that the LCR proceeds through concerted reaction without any contribution of radical species. In 2007, Yamamoto and Akiba reported the LCR using all the possible compounds of $Ar_nTol_{5-n}Sb$ (Ar = *p*-trifluoromethylphenyl, Tol: *p*-methylphenyl; n = 0-5) as starting materials and found that the LCR takes place after equilibration among possible $Ar_nTol_{5-n}Sb$ by LER in solution at high temperature[6]. In 2014, Akiba and Kobayashi published theoretical investigation on the LER of hypervalent antimony and tellurium compounds[7].

According to the apicophilicity rule, Ar ligand in $Ar_nTol_{5-n}Sb$ prefers to occupy an apical (ap) position rather than an equatorial (eq) one, which was experimentally confirmed from the X-ray structure ("ap" and "eq" define as "apical" and "equatorial", respectively). They also carried out flash vacuum thermolysis of $Ar_nTol_{5-n}Sb$ at ca. 300 °C[6], certifying that

the LCR should be an intramolecular process. Table 1 shows the yields of biaryls[6a]. Based on the apicophilicity rule and the data in Table 1, which indicates that there could not be found any bitolyl as a product, they proposed that the mechanism of LCR of $Ar_nTol_{5-n}Sb$ should be ap-ap coupling such as shown in Scheme 1. The LCRs of hypervalent compounds have also attracted theoretical chemists[8]. Moc and Morokuma reported the detailed computational study on the reactions of H_5Sb as well as H_5P, H_5As, and H_5Bi[9]. They adopted two different levels of theories, the Hartree-Fock (HF) and the second-order Møller-Plesset perturbation (MP2) theories, and then obtained different transition-state (TS) structures for the LCR of H_5Sb: ap-eq coupling from HF calculation while eq-eq coupling from more accurate MP2 calculation, both of which are different from the mechanism proposed by the experimentalists.

Table 1. Yields of biaryls by flash vacuum thermolysis of Ar*n*Tol$_{5-n}$Sb (*n* = 1-4) at ca. 300 °C[6a].

Compound	Statistical ratio			Experimental ratio		
	Ar–Ar	Ar–Tol	Tol–Tol	Ar–Ar	Ar–Tol	Tol–Tol
Ar_4TolSb	60	40	0	76 ± 2.3	24 ± 2.3	0
Ar_3Tol_2Sb	30	60	10	58 ± 1.9	42 ± 1.9	0
Ar_2Tol_3Sb	10	60	30	36 ± 1.5	64 ± 1.5	0

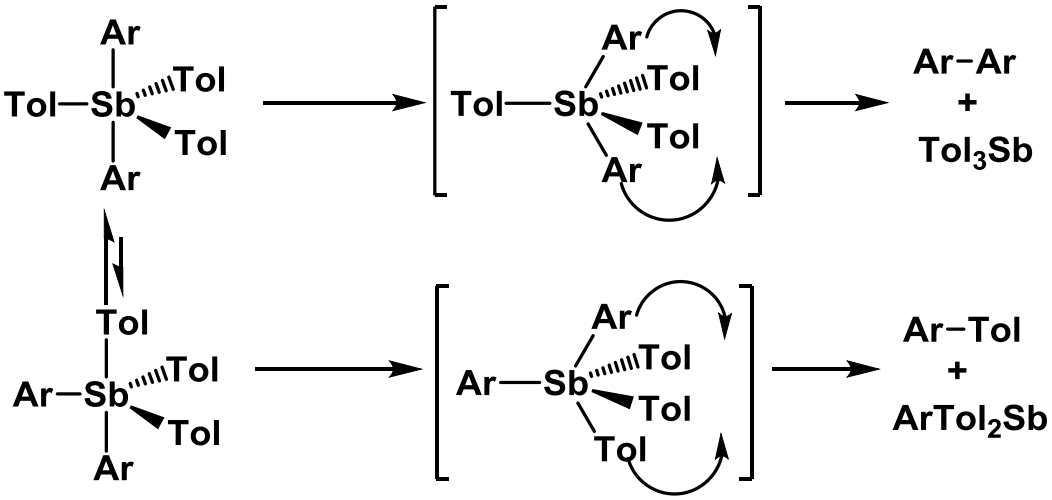

Scheme 1. Mechanism for the apical-apical (ap-ap) LCR of pentaarylantimony compounds (extracted from Ref. 6a).

2.2 Purpose

The theoretical analysis of the coupling reaction of the pentavalent antimony compound has been conducted, but the ligand is a hydrogen atom. However, the sizes of the theoretical ligands are quite different from those of experiments. The examples studied using the experimental system have been carried out by ligand exchange reaction[7]. However, there was no example of theoretical research on coupling. Therefore, solving the difference is the goal between the experimental proposal found in the introduction so far and the result obtained by the theoretical calculation.

There is a preference of arrangement of pentavalent antimony compounds by ligands (i.e. apicophilicity). Therefore, when I reveal the mechanism of the coupling, I extend the application as an intermediate in synthesizing the aimed compounds.

In addition, in order to resolve the inconsistency between the experimental results and the theoretical calculations, I theoretically investigated the mechanism of the LCR of $Ar_nTol_{5-n}Sb$ and the explored potential energy surface of H_5Sb.

2.3 Computational Details

2.3.1 General Considerations

Geometries of all compounds presented in this chapter were optimized using density functional theory (DFT) with the long-range-corrected BLYP (LC-BLYP) exchange-correlation functional[10] unless otherwise noted. All geometry optimizations were carried out using Gaussian09 package[11]. The reactant and product connected from each TS were confirmed by calculating the intrinsic reaction coordinate (IRC) pathway[12]. As for the basis set, the correlation consistent polarized valence double zeta (cc-pVDZ) basis set of Dunning[13] was adopted for H, C, and F atoms, while the pseudopotential cc-pVDZ (cc-pVDZ-pp) set[14] was adopted for Sb atoms unless otherwise noted.

2.3.2 Mulliken Population and Energy Density Analysis

Mulliken population analysis[15] has been widely used to analyze the atomic net charge. In this analysis, the number of electrons on atom *A* is estimated as:

$$q^A = \sum_{\mu \in A} \sum_{\nu} D_{\mu\nu} S_{\nu\mu} \tag{2.1}$$

where μ and ν refer to the atom-centered basis functions (so-called atomic orbitals), and **S** is the overlap integral, and **D** is density matrix, respectively. In analogy with the Mulliken population, Nakai proposed an energy density analysis (EDA) that partitions the total energy of the system into atomic contributions[16]. For example, the kinetic energy contribution from atom *A* is evaluated with the kinetic energy integral matrix **T** as:

$$E_{kin}^A = \sum_{\mu \in A} \sum_{\nu} D_{\mu\nu} T_{\nu\mu} \tag{2.2}$$

E_{kin}^{A} is occasionally referred to as the kinetic energy density for atom *A*. By applying similar formulations to all energy terms, the total energy density can be defined for each atom. The EDA program was implemented into GAMESS package[17] and used to investigate the origin of the energy stabilization.

2.3.3 Calculations of H_5Sb

Before exploring the potential energy surface of the LCR of H_5Sb, I adopted multiple methods and compared the performances of the calculations for H_5Sb monomer. The details are described in the section 2.4.5.

2.4 Results and Discussions

2.4.1 Equilibrium and TS Structures of $Ar_nTol_{5-n}Sb$ (n = 0-5)

First, I performed the geometry optimizations of the reactants, $Ar_nTol_{5-n}Sb$ (n = 0-5), all of which show trigonalbipyramidal structures, consistent with experimental results. As an example, the stable structure of Tol_5Sb (i.e., n = 0) was shown in Figure 1a. Accordingly, five ligands can be classified into two apical (ap) and three equatorial (eq) ones, where the C atoms linked to Sb (*ipso* carbons) are labeled as {C_{a1}, C_{a2}} and {C_{e1}, C_{e2}, C_{e3}}, respectively. The optimized and experimental bond lengths of the Tol_5Sb reactant are summarized in the second and third columns of Table 2, respectively. Because C_{a1}, Sb, and C_{a2} form a 3c-4e bond, the Sb–C_{a1} and Sb–C_{a2} bonds are longer and weaker than the other Sb–C_e ones. From this structure, LCR pathways were searched by shortening the lengths between two ipso C atoms. Regardless of the small configuration change, only one TS for LCR could be essentially found, of which the schematic structure and the bond lengths are given in Figure 1b and in the fourth column of Table 2, respectively. In Figure 1b, the ipso carbons of two coupling ligands are labeled as C_{a1} and C_{e1} at the reactant structure. Contrary to the proposal from the experiment[6], this TS corresponds to the ap-eq coupling, for which the coupling product forms a covalent bond between C_{a1} and C_{e1}. Correspondingly, at the TS structure, the C_{a1}–C_{e1} length was shortened to 2.049 Å from 3.101 Å at the reactant. Sb–C_{a1} length was elongated from 2.218 to 2.771 Å, while all the other Sb–C bonds are slightly but oppositely shortened, especially Sb–C_{e1} length, which is dissociated at the product, was shortened from 2.140 to 2.049 Å. This trend originates from a positive charge generated at the Sb. In Table 2, the bond lengths for the product structure are also given in the last column. The residual product (Tol_3Sb) shows the

trigonal-pyramidal structure, where three ligands are identical.

For the other reactants, $Ar_nTol_{5-n}Sb$ (n = 1-5), the reactant, TS, and product structures were obtained as well. Because there are several configurational (ap or eq) isomers for n = 1-4, I examined all conceivable reaction pathways from the possible reactant configurations. When the ligand positions of the reactant should clearly be expressed, I use the square bracket, within which the position(s) of all Ar ligand(s) are listed. For example, there are two $ArTol_4Sb$ isomers, i.e., $ArTol_4Sb$[ap] and $ArTol_4Sb$[eq]. Comparing the energies for these two isomers, $ArTol_4Sb$[ap] is ca. 5 kJ mol^{-1} more stable than $ArTol_4Sb$[eq]. This result is consistent with the apicophilicity rule or the X-ray structure of $ArTol_4Sb$[6]. For the other reactants (n = 2-4), the most stable structures are Ar_2Tol_3Sb[ap, ap], Ar_3Tol_2Sb[ap, ap, eq], and Ar_4TolSb[ap, ap, eq, eq], all of which are consistent with the X-ray structures[6]. The obtained TS structures for LCRs of these reactants are qualitatively the same as that for Tol_5Sb. Therefore, it was predicted that the LCRs of $Ar_nTol_{5-n}Sb$ (n = 0-5) proceed by the ap–eq coupling mechanism. To define the reaction pathway (or TS, equivalently), the coupling product should be specified as well as the reactant.

Table 2. Optimized bond lengths (in Å) for reactant, TS, and product structures for LCR of Tol_5Sb.

Bond	Reactant	(exptl.)[23]	TS	Product
Sb–C_{a1}	2.218	(2.254)	2.771	—
Sb–C_{a2}	2.217	(2.238)	2.112	2.132
Sb–C_{e1}	2.140	(2.145)	2.049	—
Sb–C_{e2}	2.122	(2.180)	2.090	2.132
Sb–C_{e3}	2.140	(2.151)	2.086	2.132
C_{a1}–C_{e1}	3.101	(—)	2.049	1.480

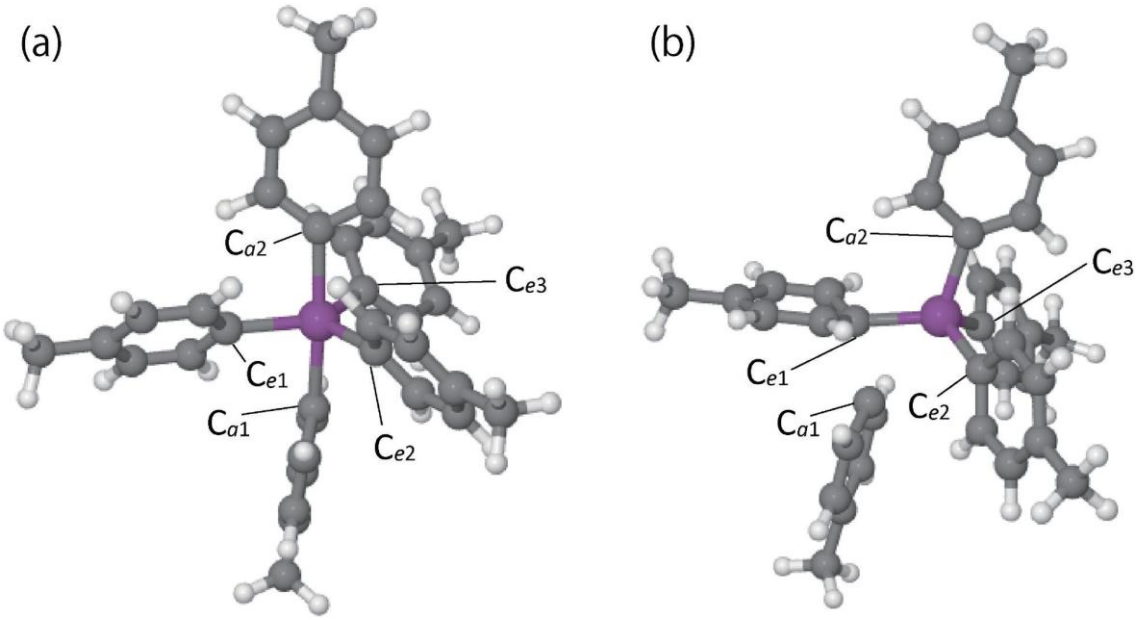

Figure 1. (a) Reactant and (b) TS structures of Tol_5Sb.

2.4.2 Energy Diagram

In this section, it is necessary to summarize the Gibbs free energy diagram for LCRs of $Ar_nTol_{5-n}Sb$ (n = 0-5) at 573.15 K. First, the reaction pathway should be expressed by denoting the coupling product after the reactant, separated by a slash (/). A coupling product consists of two ligands, one of which is from ap position and the other from eq. Then, the notation for a product A–B was used in which A is from ap and B is from eq position. Considering the LCR of Ar_2Tol_3Sb, for example, there are seven conceivable pathways: i.e. Ar_2Tol_3Sb[ap, eq]/Ar–Ar, Ar_2Tol_3Sb[ap, eq]/Tol–Ar, Ar_2Tol_3Sb[eq, eq]/Tol–Ar, Ar_2Tol_3Sb[ap, ap]/Ar–Tol ,Ar_2Tol_3Sb[ap, eq]/Ar–Tol, Ar_2Tol_3Sb[ap, eq]/Tol–Tol, and Ar_2Tol_3Sb[eq, eq]/Tol–Tol. The chemical formula of the reactant is omitted to obviously understand of the energy diagrams.

When considering the LCR of Ar_2Tol_3Sb as a typical example, where seven different pathways defined by the reactant configuration and the coupling product are possible. The energy diagrams for these LCR pathways of Ar_2Tol_3Sb are shown in Figure 2. Throughout this paper, the energy of the most stable reactant, Ar_2Tol_3Sb[ap, ap] in this case, was set to be 0 of the relative energy. The energy of Ar_2Tol_3Sb[eq, eq], which is the most unstable reactant, is 13.4 kJ mol^{-1} higher than Ar_2Tol_3Sb[ap, ap]. Compared to the TS energy (195 kJ mol^{-1} at the lowest), the energy difference among the reactant configurations is negligibly small and these configurations are thermally equilibrated quite rapidly when occurring LCR. The TS energy is mostly determined by the kinds of coupling products: ca. 247, 228, 210, and 195 kJ mol^{-1} for Tol–Tol, Ar–Tol, Tol–Ar, and Ar–Ar product, respectively. This result can qualitatively explain the experimental fact that the yield of Ar-Ar product (36%) is considerably higher than the simple statistical estimate (10%) and that Tol–Tol product cannot be obtained (Table 1). The reason for the tendency of TS

energies will be investigated later. The energy of the product is ca. 350 kJ mol^{-1} lower than the reactant.

The energy diagrams were obtained for the other reactants as well, which are shown in Figures 3-6. The conclusion is essentially the same; (1) the energy differences among the reactant and product configurations are sufficiently small compared to those at the TS energy and (2) the TS energy is mostly determined by the coupling product and the order is Ar–Ar < Tol–Ar < Ar–Tol < Tol–Tol. Therefore, I find that the yield of the product of LCR is determined kinetically and is independent of the stability of the reactant.

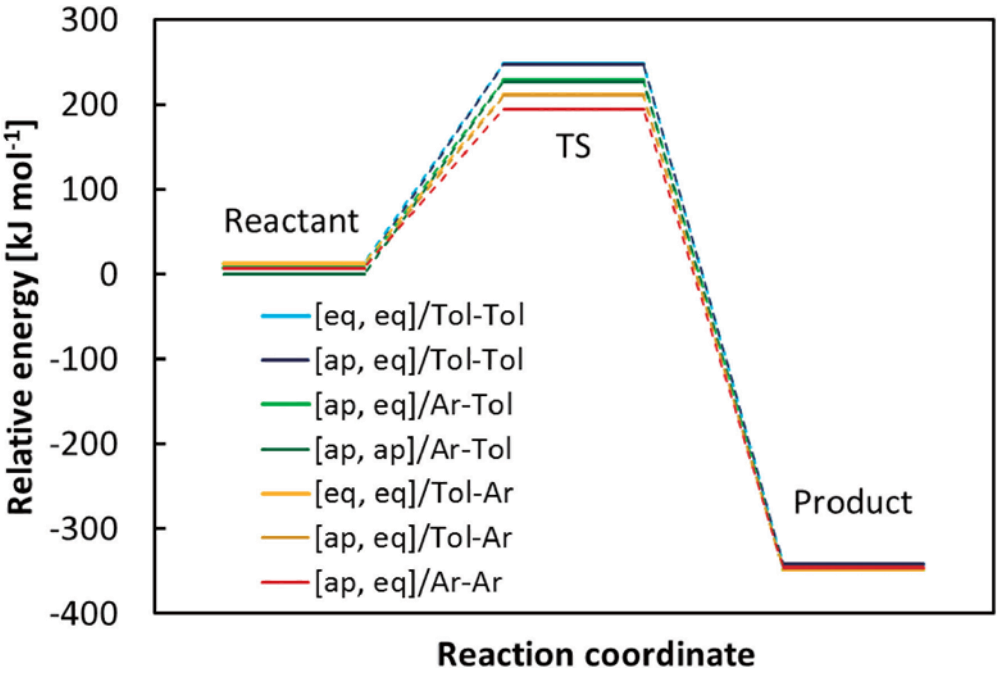

Figure 2. The energy diagram for LCR of Ar_2Tol_3Sb.

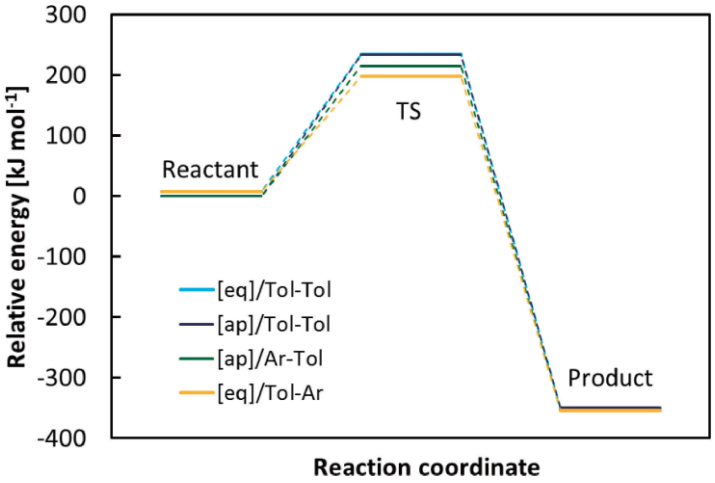

Figure 3. The energy diagram for LCR of $ArTol_4Sb$.

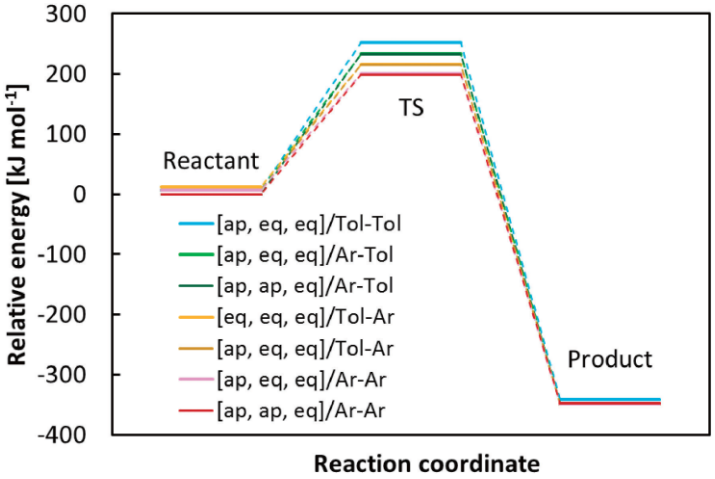

Figure 4. The energy diagram for LCR of Ar_2Tol_3Sb.

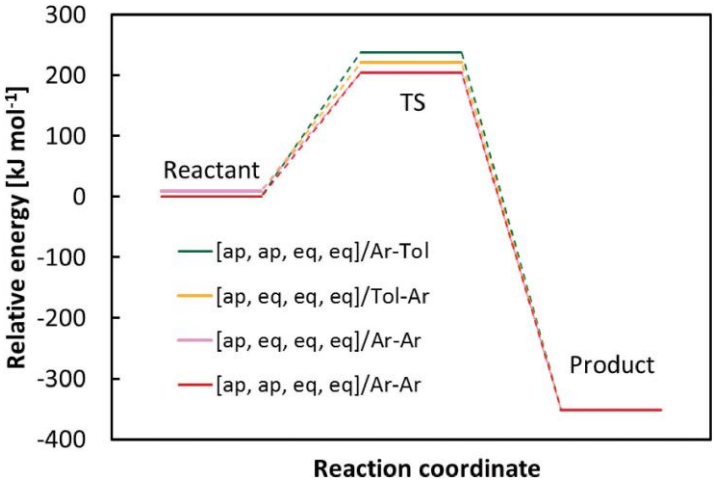

Figure 5. The energy diagram for LCR of Ar_4TolSb.

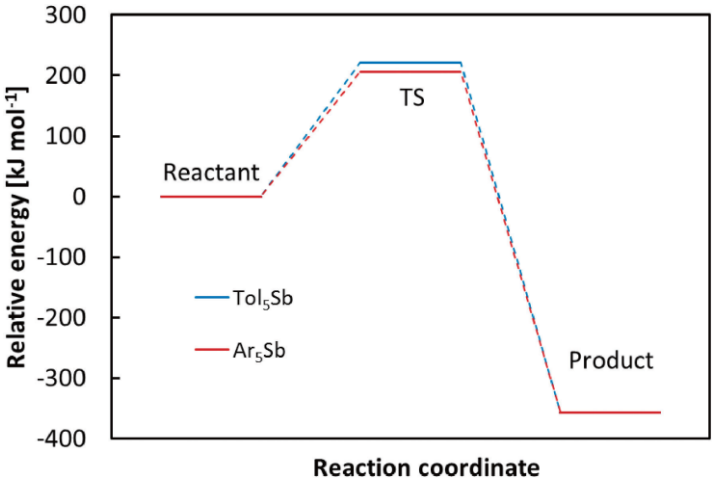

Figure 6. The energy diagram for LCRs of Ar_5Sb and Tol_5Sb.

2.4.3 Energy Density Analysis

From here, the reason for the large energy differences among the TS structures (in other words, I investigated the stability of the TS for the Ar–Ar production). First, I performed the EDA for four TS structures from Ar_2Tol_3Sb[ap, eq]. Table 3 summarizes the change of energy density from the reactant to the TS structure. Because EDA cannot be applied to the thermal correction energies, the sum of the electronic energy and nuclear repulsion energy in this subsection were considered. Using EDA, the total energy is divided into four fragments: the Sb atom, coupling ap ligand, coupling eq ligand, and the other ligands. Positive (negative) value indicates that the component at the TS structure is destabilized (stabilized) from the reactant. At the TS structure, shown in Figure 1b for Tol_5Sb, the coupling ap ligand is partially detached slantwise from Sb. Because the coupling ap ligand forms the 3c-4e bond with Sb and the other ap ligand at the reactant structure, the 3c-4e (bonding and nonbonding) orbitals will be reconstructed to the usual single bond and lone-pair orbitals at the TS structure:

$$\text{3c-4e R–Sb–R}^{*} \rightarrow \text{R–Sb}^{+} + :\text{R}^{*-}$$

where R^{*} denotes the coupling ap ligand. Therefore, to estimate the destabilization by the bond cleavage of SbR^{*}, the sum of the energy changes for Sb and R will be a good indicator, which is also listed in Table 3. The largest energy change of destabilization appears on Sb atom because the Sb atom formally has +1 charge at the TS structure. On the other hand, the coupling ap ligand (R^{*}) is stabilized due to its anionic picture. The sum of these two contributions comes up to +106.6-120.8 kJ mol^{-1}, namely, when the coupling ap ligand is Ar, the destabilization energy is ca. 7 kJ mol^{-1} smaller than when the ligand is Tol. Instead, the destabilization energy of the coupling eq ligand shows a good correlation with the activation energy. Namely, when the coupling eq ligand is Ar,

the destabilization energy is ca. 25 kJ mol^{-1} smaller than its Tol ligand counterpart. I have found that the stability of the coupling eq ligand is important to lower the activation energy.

Table 3. Energy density changes (in kJ mol^{-1}) of the TS structures from Ar_2Tol_3Sb[ap,eq] reactant.

Component	Coupling product (ap–eq)			
	Ar–Ar	Tol–Ar	Ar–Tol	Tol–Tol
Sb + coupling ap ligand	+106.6	+114.0	+113.2	+120.8
(Sb atom)	(+164.6)	(+149.8)	(+187.8)	(+172.6)
(coupling ap ligand)	(–58.0)	(–35.8)	(–74.6)	(–51.8)
Coupling eq ligand	+14.2	+20.4	+40.6	+47.2
The other ligands (sum)	+65.8	+67.2	+67.4	+70.1
Activation energy	+186.6	+201.7	+221.2	+238.0

Positive (negative) value indicates that the component in the TS structure is destabilized (stabilized) from the reactant. The sum of electronic and nuclear repulsion energies is partitioned into the components by EDA. The activation energy here does not include any thermal corrections.

2.4.4 Frontier Orbital Analysis

By using EDA, it was suggested that the coupling eq Ar ligand at the TS structure is relatively more stabilized than the coupling eq Tol ligand by ca. 25 kJ mol^{-1}. In addition, I confirmed from the TS structure depicted in Figure 1b that the benzene ring in the coupling eq ligand lies almost vertically to the lone-pair orbital in the coupling ap ligand. Therefore, the interaction between the lone-pair orbital (n) of the coupling ap ligand and the π^* orbital of the coupling eq ligand should exist and may play an important role to determine the stability of the TS structure. The left-hand side of Figure 7 shows the highest occupied molecular orbital (HOMO) at the TS structure for Ar_2Tol_3Sb[ap, eq]/Ar–Ar pathway. The orbitals for Ar^- and ArTol3Sb^+ were also obtained at this structure, for which the HOMO (= nonbonding orbital: n) of Ar^- and the lowest unoccupied molecular orbital (LUMO = π^*) of $ArTol_3Sb^+$ are depicted on the right-hand side of Figure 7. Obviously, the HOMO of the TS structure is formed by the n–π^* interaction.

Table 4 lists the HOMO energies for four TS structures together with the activation free energies. There exists a clear correlation between the HOMO energy and the activation energy. Because of the electron-withdrawing CF_3 group, the π^* orbital of the equatorial Ar ligand has lower energy than that of Tol ligands. Actually, the LUMO of the equilibrium Ar_2Tol_3Sb[ap, eq] structure is localized on the equatorial Ar ligand. Therefore, the HOMO at the TS structure, which is constructed by the interaction between the apical n orbital and the equatorial π^* orbital, is more stabilized for the LCR with the equatorial Ar ligand than with the Tol ligand, and the activation energies for this type of LCRs become lower.

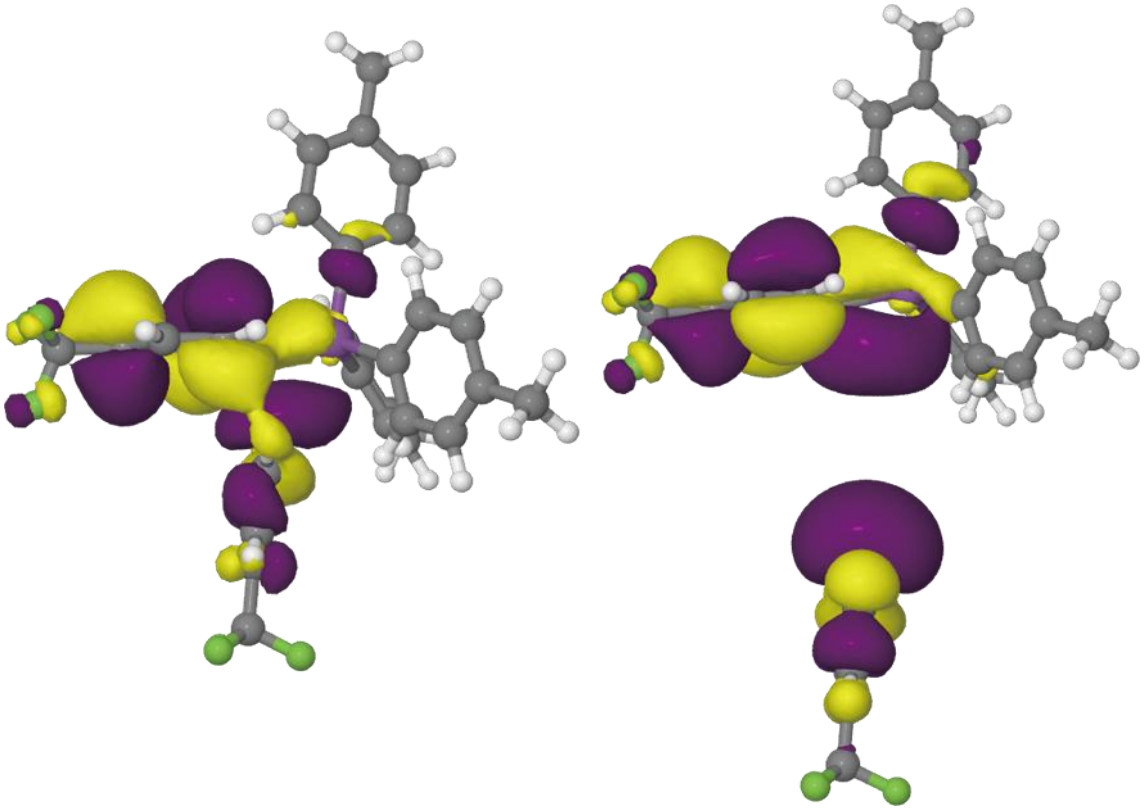

Figure 7. HOMO of the TS ($[Ar^{-}\cdots ArTol_3Sb^{+}]^{‡}$) structure for producing Ar_2 (left). This orbital is formed by the interaction between $[ArTol_3Sb^{+}]^{‡}$ LUMO (right upper) and $[Ar^{-}]^{‡}$ HOMO (right lower).

Table 4. Activation free energies ($\Delta G^{‡}$) and the HOMO energies of the corresponding TS structures for LCRs of Ar_2Tol_3Sb[ap,eq].

Product (ap-eq)	HOMO energy [eV]	$\Delta G^{‡}$ [kJ mol^{-1}]
Ar-Ar	–6.34	194.2
Tol-Ar	–6.26	209.6
Ar-Tol	–5.85	228.8
Tol-Tol	–5.75	247.0

2.4.5 Optimization of H_5Sb

Moc and Morokuma reported the TS structure for the elimination of H_2 from H_5Sb[9]. They obtained TS for eq-eq coupling when calculating at the spin-restricted MP2 level with LanL2DZ plus Huzinaga polarization set, while they obtained TS for ap-eq coupling when calculating by the low-level (spin-restricted HF) method with the same basis set.

As shown above, the quantum chemical studies suggest ap-eq coupling for LCR of $Ar_nTol_{5-n}Sb$. Here, I investigate the potential energy surface of the H_5Sb system and reconsider the LCR pathway for this system.

Before exploring the potential energy surface, I assessed the performance of the present LC-BLYP/cc-pVDZ(-pp) level of theory for this system through comparisons with the results by the other DFT functionals [namely, B3LYP (Refs. [10, 18]) and M06 (Ref. [19])] and by the coupled cluster (CC) theory [namely, CCSD and CCSD(T) methods][20]. In the CC calculations, the triple zeta quality basis set, referred to as cc-pVTZ(-pp)[13, 14], was adopted. Three characteristic structures, shown in Figure 8; namely, the equilibrium structure (EQ), the transition state for pseudorotation (TS1), and the transition state for LCR (TS2) structures, are optimized. The labels for hydrogen atoms are also given in this Figure. Table 5 lists the geometric parameters of H5Sb optimized by LC-BLYP/cc-pVDZ(-pp), B3LYP/cc-pVDZ(-pp), M06/cc-pVDZ(-pp), CCSD/cc-pVTZ(-pp), and CCSD(T)/cc-pVTZ(-pp) calculations. The structures obtained from CCSD and CCSD(T) calculations are very close to each other. As for the DFT results, the structures obtained by LC-BLYP calculations show very good agreement with those by CCSD(T) calculations: the root mean square deviations of the LC-BLYP geometry from CCSD(T) one for EQ, TS1, and TS2 structures are 0.007, 0.005, and 0.038 Å, respectively, which are smaller than B3LYP (0.020, 0.019, and 0.077 Å) or M06 (0.017, 0.017, and 0.146 Å)

results. Table 6 compares the activation energies for pseudorotation [*E*(TS1)–*E*(EQ)] and LCR [*E*(TS2)–*E*(EQ)] among LCBLYP, CCSD, and CCSD(T) calculations. Here, the thermally corrected Gibbs free energies using the harmonic approximation are given together except for CCSD(T), for which the analytical Hessian code is not implemented in Gaussian. Although the activation energies obtained from the LC-BLYP calculation are slightly higher than those from CCSD(T), they are comparable to CCSD results. By this comparison, I concluded that the LC-BLYP/cc-pVDZ(-pp) level of theory is applicable to explore the potential energy surface of this system.

Table 5. Geometric parameters for equilibrium and transition-state structures of H_5Sb molecule optimized at LC-BLYP/cc-pVDZ(-pp), B3LYP/cc-pVDZ(-pp), M06/cc-pVDZ(-pp), CCSD/cc-pVTZ(-pp), and CCSD(T)/cc-pVTZ(-pp) levels.

Structure	Parameter	LC-BLYP/ cc-pVDZ	B3LYP/ cc-pVDZ	M06/ cc-pVDZ	CCSD/ cc-pVTZ	CCSD(T)/ cc-pVTZ
Equilibrium	R(Sb–H_1)/Å	1.696	1.726	1.723	1.702	1.705
	R(Sb–H_4)/Å	1.764	1.785	1.782	1.760	1.762
	R(H_2–H_3)/Å	2.941	2.991	2.987	2.948	2.953
TS1	R(Sb–H_1)/Å	1.666	1.689	1.690	1.671	1.673
(pseudorotation)	R(Sb–H_2)/Å	1.740	1.766	1.763	1.741	1.744
	A(H_1–Sb–H_2)/°	101.6	101.2	101.3	101.6	101.4
	A(H_2–Sb–H_4)/°	87.7	87.8	87.8	87.7	87.7
TS2 (LCR)	R(Sb–H_1)/Å	1.738	1.779	1.779	1.742	1.745
	R(Sb–H_2)/Å	1.745	1.755	1.740	1.755	1.763
	R (Sb–H_3)/Å	1.858	1.924	1.969	1.868	1.868
	R(Sb–H_4)/Å	1.689	1.714	1.708	1.697	1.702
	R(H_2–H_3)/Å	1.381	1.477	1.496	1.383	1.392
	A(H_1–Sb–H_2)/°	163.0	162.6	158.1	167.3	168.4
	A(H_1–Sb–H_3)/°	152.1	150.4	154.8	147.9	146.6
	A(H_1Sb–H_4)/°	93.6	93.1	93.5	93.3	93.3
	A(H_4–Sb–H_5)/°	156.2	149.7	144.1	154.1	154.5

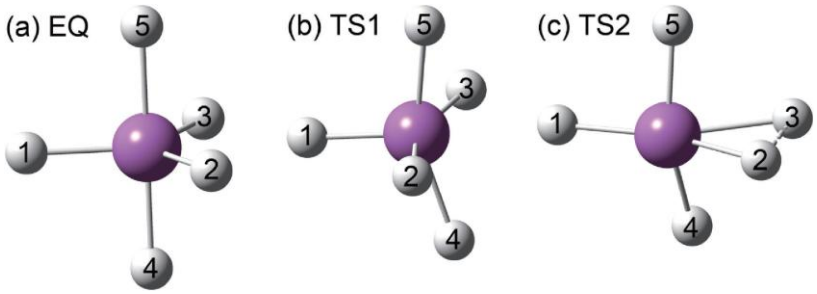

Figure 8. EQ (D_{3h}), TS1 (C_4), TS2 (C_s) structures of H_5Sb. The numbers on H atoms are used as the labels. Sb, H1, H2, and H3 lies on the symmetry plane.

Table 6. Comparison of uncorrected ($\Delta E^{\ddagger}$) and thermal corrected ($\Delta G^{\ddagger}$) activation energies (in kJ mol^{-1}) of H_5Sb among LC-BLYP/cc-pVDZ(-pp), CCSD/cc-pVTZ(-pp), and CCSD(T)/cc-pVTZ(-pp) calculations (The geometries were also optimized at the same level of theory).

	Reaction	LC-BLYP/ cc-pVDZ(-pp)	CCSD/ cc-pVTZ(-pp)	CCSD(T)/ cc-pVTZ(-pp)
Uncorrected	Pseudorotation	+9.6	+9.1	+8.4
	LCR	+155.8	+152.7	+143.9
Thermal corrected (298.15 K)	Pseudorotation	+6.8	+6.0	
	LCR	+147.0	+142.0	

2.4.6 LCR of H_5Sb

To examine the reaction mechanism for the elimination of H_2 from H_5Sb involving both LCR and pseudorotation, a two-dimensional potential energy surface was determined in terms of H_1–Sb–H_2 and H_1–Sb–H_3 bond angles (denoted as θ_1 and θ_2, respectively), where all the other geometric parameters were optimized under the *Cs* symmetry constraint. Note that all the three structures of EQ, TS1, and TS2 have a symmetry plane that contains Sb, H_1, H_2, and H_3 as shown in Figure 8. A contour plot of the calculated potential energy surface is shown in Figure 9. Gray circle symbols correspond to the EQ structures. For example, on the point of (θ_1, θ_2) = (120 °, 120 °), H_1, H_2, and H_3 are at the equatorial positions, while H2 and H3 are at the apical positions on (θ_1, θ_2) = (90 °, 90 °). Square symbols represent the TS structures, namely, three squares between two EQ structures correspond to TS1, and two squares at (θ_1, θ_2) = (163 °, 152 °) and (θ_1, θ_2) = (152 °, 163 °) correspond to TS2. Upper right corner of this Figure, where the potential energy is below –50 kJ mol^{-1}, corresponds to the product, H_2 + H_3Sb. Dashed lines between EQ and TS structures are the IRC pathways projected onto this θ_1–θ_2 plane, calculated by using GAMESS program[17] with the linear gradient following method. The IRCs from TS2 are connected to the EQ at (θ_1, θ_2) = (120 °, 120 °), indicating the occurrence of the eq-eq coupling. Because of the molecular symmetry, TS2 structures also appear at (θ_1, θ_2) = (163 °, 45 °), (152 °, 45 °), (45 °, 163 °), and (45 °, 152 °), all of which connect with the EQ at (θ_1, θ_2) = (120 °, 120 °) by the IRC pathways. The TS2 structures connected with the other EQs do not exist on the θ_1–θ_2 plane. Note that although the two IRCs from TS2 in Figure 9 seem to cross each other, this crossing does not occur on the 3N–6 dimensional potential energy hypersurface, because the IRC pathways are not on the lowest energy surface of the θ_1–θ_2 plane.

To investigate the effect of pseudorotation of H_5Sb on the H_2-elimination pathway, vibrational frequencies of transverse normal modes orthogonal to the IRC were calculated along the IRC pathway from TS2 to EQ. Then, it is found that the lowest eigenvalue of the projected Hessian matrix changes its sign from positive to negative just after passing TS2, indicating appearance of the valley-ridge transition (VRT) point along the IRC[21]. In Figure 9, VRT points are represented by diamond symbols while a direction of the transverse vibrational mode with zero curvature at VRTs projected onto the θ_1–θ_2 plane is depicted by the green arrows. Obviously, these arrows direct to the EQs at (θ_1, θ_2) = (180 °, 90 °) and (90 °, 180 °), indicating that the ap-eq coupling is also possible even for H_5Sb system. Therefore, I can conclude that there is no inconsistency with our results for LCR of $Ar_nTol_{5-n}Sb$.

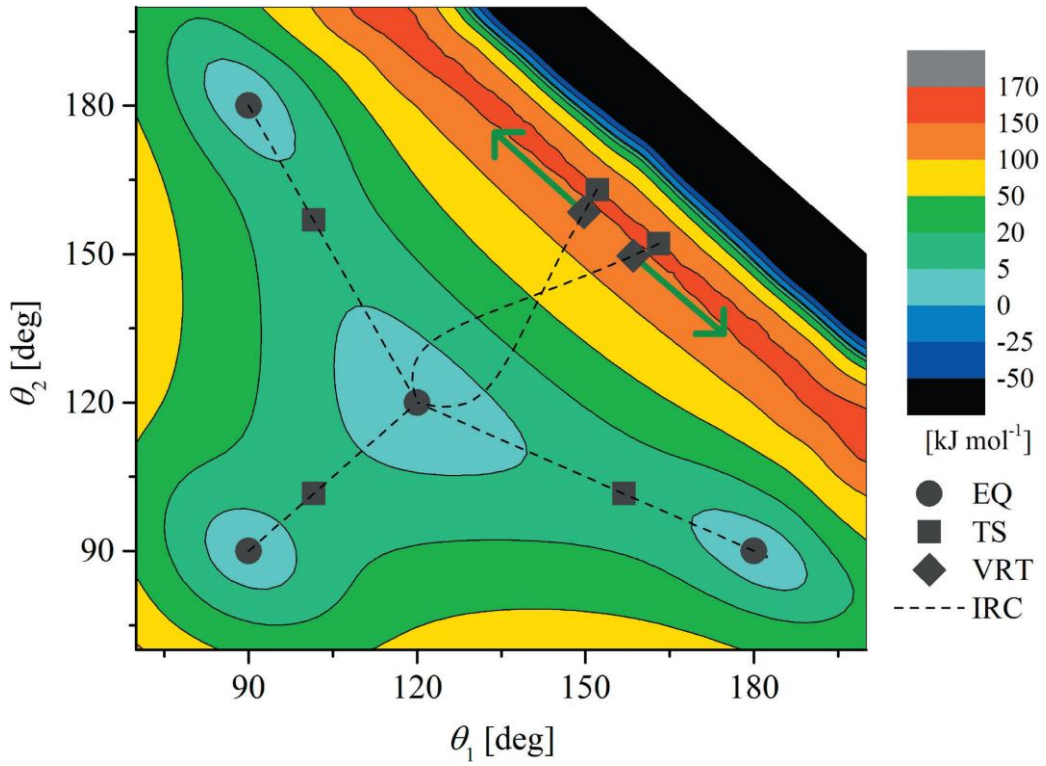

Figure 9. Potential energy surface of H_5Sb on C_s structure at LC-BLYP/cc-pVDZ(-pp) level. θ_1 and θ_2 represent H1–Sb–H2 and H1–Sb–H3 angles, respectively, where Sb, H1, H2, and H3 lie on the symmetry plane as shown in Figure 8. Gray circle (●) and square (■) symbols represent the equilibrium (EQ) and the transition state (TS) structures, respectively. Dashed lines show the intrinsic reaction coordinate (IRC) pathways projected onto the θ_1 θ_2 plane and diamond (◆) symbols correspond to the valley-ridge transition (VRT) points found on IRC pathways. At VRT points, the direction of the transverse vibrational mode with zero curvature is depicted by green arrows.

2.5 Conclusion

Experimental studies of the ligand coupling reactions (LCRs) of pentacoordinate antimony compounds of $Ar_nTol_{5-n}Sb$ have suggested the ap-ap coupling mechanism. In the present DFT [LC-BLYP/cc-pVDZ(-pp)] study of $Ar_nTol_{5-n}Sb$, I found that the LCRs of these compounds proceed with the ap-eq coupling mechanism. The experimental product ratio could be explained by the difference of activation energy for each combination of ap-eq ligands. The energy density and the frontier orbital analyses revealed that the stability of the HOMO at the TS structure, which is formed by the interaction between the lone-pair (n) orbital of the coupling ap ligand and the π^* orbital of the coupling eq ligand, is important to decrease the activation energy. Furthermore, the potential energy surface of H_5Sb was investigated in detail at the same level of computation, of which the results showed good agreement with those by the ab initio CCSD/cc-pVTZ(-pp) level. I confirmed that the IRC from the TS structure for LCR supports the eq-eq coupling mechanism, as reported by Moc and Morokuma with the MP2 method. However, the valley-ridge transition (VRT) point was found on the IRC close to the TS structure. The direction of the vibrational mode orthogonal to IRC having a negative curvature near the TS structure showed that there exists ap-eq coupling reaction path even for the LCR of H_5Sb. This research would offer the clue to apply the LCR as a method to synthesize the biaryls.

I have already published two papers about the result of this chapter[22].

2.6 References

1. a) Chemistry of Hypervalent Compounds, ed. by K. Akiba, Wiley-VCH, New York, **1999**; b) K. Akiba, Organo Main Group Chemistry, John Wiley & Sons, Hoboken, **2011**; c) J.-P. Finet, Ligand Coupling Reactions with Heteroatomic Compounds, Elsevier Science, Oxford, UK, **1998**.
2. A. L. Beauchamp, M. J. Bennett, F. A. Cotton, *J. Am. Chem. Soc.* **1968**, *90*, 6675.
3. For example, a) M. Nakamoto, S. Kojima, S. Matsukawa, Y. Yamamoto, K.-y. Akiba, *J. Organomet. Chem.* **2002**, *643-644*, 441; b) R. S. McDowell, A. Streitwieser, Jr., *J. Am. Chem. Soc.* **1972**, *94*, 3047.
4. R. S. Berry, *J. Chem. Phys.* **1960**, *32*, 933.
5. K.-W. Shen, W. E. McEwen, A. P. Wolf, *J. Am. Chem. Soc.* **1969**, *91*, 1283. M. Kobayashi, K. Akiba, *Organometallics* **2014**, *33*, 1218.
6. a) R. Hoffmann, J. M. Howell, E. L. Muetterties, *J. Am. Chem. Soc.* **1972**, *94*, 3047; b) W. Kutzelnigg, J. Wasilewski, *J. Am. Chem. Soc.* **1982**, *104*, 953.
7. M. Kobayashi, K. Akiba, *Organometallics* **2014**, *33*, 1218. J. Moc, K. Morokuma, *J. Am. Chem. Soc.* **1995**, *117*, 11790.
8. a) G. Schröder, T. Okinaka, Y. Mimura, M. Watanabe, T. Matsuzaki, A. Hasuoka, Y. Yamamoto, S. Matsukawa, K. Akiba, *Chem. Eur. J.* **2007**, *13*, 2517; b) K. Akiba, *Pure Appl. Chem.* **1996**, *68*, 837.
9. J. Moc, K. Morokuma, *J. Am. Chem. Soc.* **1995**, *117*, 11790.
10. a) H. Iikura, T. Tsuneda, T. Yanai, K. Hirao, *J. Chem. Phys.* **2001**, *115*, 3540; b) A. D. Becke, *Phys. Rev. A* **1988**, *38*, 3098.
11. M. J. Frisch, G. W. Trucks, H. B. Schlegel, G. E. Scuseria, M. A. Robb, J. R. Cheeseman, G. Scalmani, V. Barone, B. Mennucci, G. A. Petersson, H. Nakatsuji,

M. Caricato, X. Li, H. P. Hratchian, A. F. Izmaylov, J. Bloino, G. Zheng, J. L. Sonnenberg, M. Hada, M. Ehara, K. Toyota, R. Fukuda, J. Hasegawa, M. Ishida, T. Nakajima, Y. Honda, O. Kitao, H. Nakai, T. Vreven, J. A. Montgomery, Jr., J. E. Peralta, F. Ogliaro, M. Bearpark, J. J. Heyd, E. Brothers, K. N. Kudin, V. N. Staroverov, T. Keith, R. Kobayashi, J. Normand, K. Raghavachari, A. Rendell, J. C. Burant, S. S. Iyengar, J. Tomasi, M. Cossi, N. Rega, J. M. Millam, M. Klene, J. E. Knox, J. B. Cross, V. Bakken, C. Adamo, J. Jaramillo, R. Gomperts, R. E. Stratmann, O. Yazyev, A. J. Austin, R. Cammi, C. Pomelli, J. W. Ochterski, R. L. Martin, K. Morokuma, V. G. Zakrzewski, G. A. Voth, P. Salvador, J. J. Dannenberg, S. Dapprich, A. D. Daniels, O. Farkas, J. B. Foresman, J. V. Ortiz, J. Cioslowski, D. J. Fox, Gaussian09 (Revision D.01), Gaussian, Inc., Wallingford, CT, **2013**.

12. a) K. Fukui, *Acc. Chem. Res.* **1981**, *14*, 363; b) H. P. Hratchian, H. B. Schlegel, in Theory and Applications of Computational Chemistry: The First Forty Years, ed. by C. E. Dykstra, G. Frenking, K. S. Kim, G. E. Scuseria, Elsevier, Amsterdam, **2005**, pp. 195-249.
13. T. H. Dunning, Jr., *J. Chem. Phys.* **1989**, *90*, 1007.
14. K. A. Peterson, *J. Chem. Phys.* **2003**, *119*, 11099.
15. R. S. Mulliken, *J. Chem. Phys.* **1955**, *23*, 1833.
16. H. Nakai, *Chem. Phys. Lett.* **2002**, *363*, 73.
17. a) M. W. Schmidt, K. K. Baldridge, J. A. Boatz, S. T. Elbert, M. S. Gordon, J. H. Jensen, S. Koseki, N. Matsunaga, K. A. Nguyen, S. Su, T. L. Windus, M. Dupuis, J. A. Montgomery, Jr., *J. Comput. Chem.* **1993**, *14*, 1347; b) M. S. Gordon, M. W. Schmidt, in Theory and Applications of Computational Chemistry: The First Forty

Years, ed. by C. E. Dykstra, G. Frenking, K. S. Kim, G. E. Scuseria, Elsevier, Amsterdam, **2005**, pp. 1167-1189.

18. A. D. Becke, *J. Chem. Phys.* **1993**, *98*, 5648.
19. Y. Zhao, D. G. Truhlar, *Theor. Chem. Acc.* **2008**, *120*, 215.
20. I. Shavitt, R. J. Bartlett, Many-Body Methods in Chemistry and Physics: MBPT and Coupled-Cluster Theory, Cambridge University Press, New York, **2009**.
21. a) P. Valtazanos, K. Ruedenberg, *Theor. Chim. Acta* **1986**, *69*, 281; b) J. Baker, P. M. W. Gill, *J. Comput. Chem.* **1988**, *9*, 465; c) Y. Harabuchi, T. Taketsugu, *Theor. Chem. Acc.* **2011**, *130*, 305.
22. a) M. Kobayashi, Y. Kuroda, K.-y. Akiba, T. Taketsugu, *Bull. Chem. Soc. Jpn.* **2015**, *88*, 1584; b) M. Kobayashi, Y. Kuroda, K.-y. Akiba, T. Taketsugu, *J. Comp. Chem. Jap.* **2015**, *14*, 199-200.
23. C. Brabant, J. Hubert, A. L. Beauchamp, *Can. J. Chem.* **1973**, *51*, 2952.

3 Dispersion and Crystal Packing of the Ultralong C–C Bond of Organic Compound

3.1 Ultralong C–C bond

3.1.1 Long C–C Bond

A general C–C bond (single bond) length is established by the sp^3–sp^3 hybrid orbital, and the length is 1.54 Å in the case of diamond, or 1.53 Å in the case of ethane. When sterically bulky substituents present around the bond, steric repulsion causes a stretch to the extent that the bond is not cleaved. Then, the bond length is often greater than 1.6 Å.

There are a number of compounds with the bonds over 1.6 Å. Compound **1** (Scheme 1) has a long C–C bond over 1.6 Å in which two adamantine skeletons are combined[1], and Compound **2** (Scheme 1) has a long C–C bond over 1.7 Å which connects a phenyl group or a *t*-butyl group to a 4-membered ring condensed with a benzene ring[2]. Both compounds have a long C–C bonds which are surrounded such bulky substituents or skeletons. On the other hand, the shortest limit distance between carbon atoms where C–C bonds do not form over 1.80 Å in X-ray crystal structure analysis of bicyclo-ring[1.1.1]pentane (Compound **3**, Scheme 1) by Wood, hence the experimental limit of a C–C bond is 1.80 Å[3].

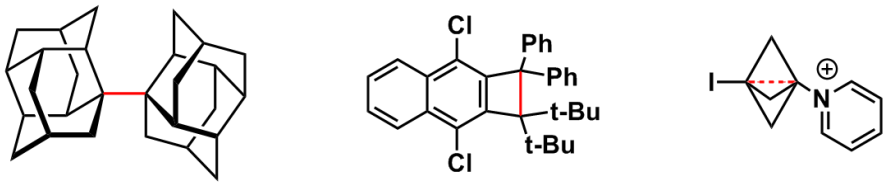

1 2 3

Scheme 1. The structures of Compound **1**-**3**. The red bond is the "long" C–C bond (Compound **1** and **2**), and the red dashed line is the C---C nonbonding line (Compound **3**).

According to the theoretical research of Zavitsas, he mentioned that the limit of C–C bond length is set to 1.748 Å[4]. This corresponds to an intercept when the bond dissociation energy (BDE) becomes 0. The C–C bond length greater than the theoretical border will have a negative BDE, which means that it cannot exist as a bond. Therefore, the experimental limit of the C–C bond length presently corresponds to the result by Zavitsas.

C=C bonds and C≡C bonds include overlap of π orbitals, so they are shortened to 1.34 Å and 1.20 Å, respectively[5]. The extension of these bonds is often observed, and there are many bonds which are reported as conjugation, because of the delocalization of electron density, which is referred to in Chapter 1. Generally, the stretches of double bonds and triple bonds are involving π orbitals. Then, there are not so many C=C bonds nor C≡C bonds which are localized and lengthened by steric repulsion. The example of compounds which has localized and long C=C bond is Compound **4** (Scheme 2). This localized C=C bond is surrounded by the "bulky" skeletons. This skeleton of Compound **4** is similar that I discuss after this section[6].

The shortest limit of the C–C bond length is shown in Compound **5** (Scheme 2), which is the relative of tetrahedranyltetrahedrane. It has a C–C bond whose length is ca. 1.436 Å[7]. It is said to derive from the high s character, according to the report. But the shortest limit is not the object in this research.

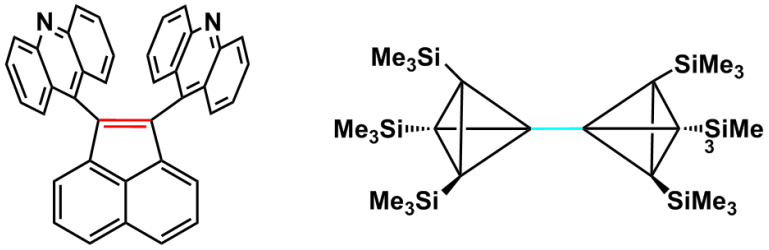

4 **5**

Scheme 2. The structures of Compound **4** and **5**. The red bond is the "long" C–C bond (Compound **4**), and the light-blue line is the shortest C–C bond (Compound **5**).

3.1.2 Hexaphenylethane

In the hexaphenylethane (HPE) skeleton (Compound **6**, Scheme 3), all H atoms around the C–C bond of ethane area are substituted to phenyl groups. There is a steric repulsion among the phenyl groups which strongly works, and the C–C bond cause radical cleavage. Radical cleavage is an equilibrium reaction, and two equivalent radicals are produced[8]. Moreover, the radical species react with each other to form a different dimer (*α*,*p*-dimer, Compound **7**, Scheme 3) from HPE. Therefore, the equilibrium of radical cleavage reaction is biased toward radical species, and HPE itself is a very unstable compound. Then, by clumping phenyl groups with each other by bonding (Scheme 4), the movable region of the substituent becomes small[9]. Then, the equilibrium of radical cleavage reaction is biased toward HPE side, radical cleavage is suppressed. This made it possible to handle neutral as HPE analog. The influence of the effect of steric repulsion remained unchanged, so the C–C bond was considered to stretch, and the bond was weakened. If skeletons like acridan skeletons are incorporated there and placed in an environment where its C–C bond can be reversibly cleaved by an external stimulus, it can be handled as a molecule controlling color change and fluorescence emission[10].

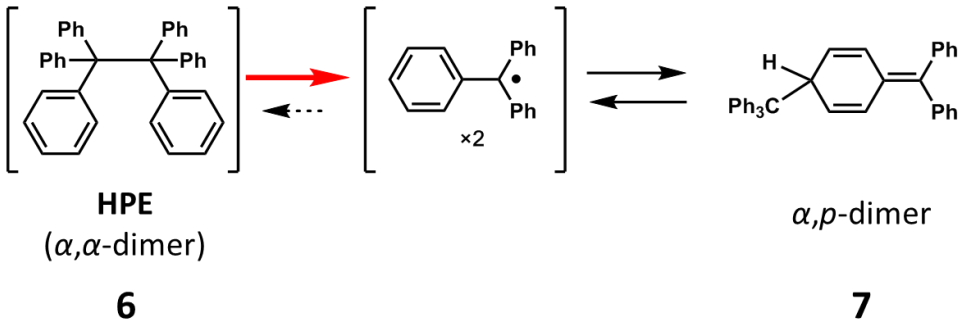

Scheme 3. The equilibrium of hexaphenylethane.

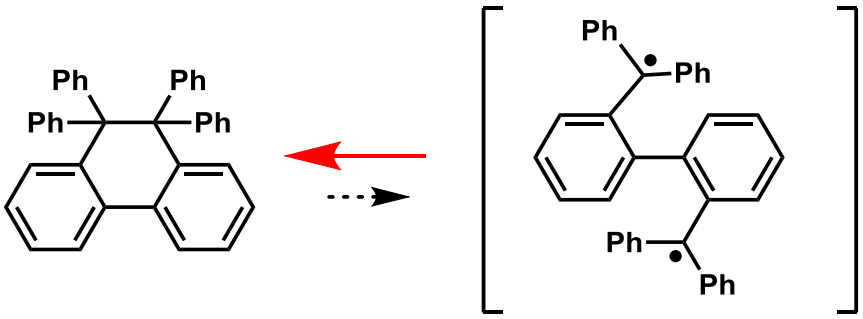

Scheme 4. The suppression of radical cleavage.

3.1.3 Dispirobis(10-methylacridane)pyracene and Derivatives

Compound **8** (Scheme 5) to be handled in this study is a compound having a long C–C bond. This compound was synthesized by Kawai, Suzuki, *et al.* in 2005 and X-ray crystal structure analyses at 93-413 K was achieved[11-13]. Compound **8** maintains the presence as a bond by using a condensed ring structure. In the X-ray crystal structure analysis at 93 K, there are 4 molecules in the unit cell, one of which has a bond showing a C–C bond length of 1.771 (3) Å (see Table 1). This value is ignoring the limit of C–C single bond proposed by Zavitsas. On the other hand, Kawai, Suzuki, and colleagues explained the validity of existence of C–C bonds from the result of two-dimensional mapping of electron density[12]. Compound **8** is known that the "ultralong C–C single bond" expands with temperature rise, and they reported that the C–C single bond stretches to 1.791 Å at 413 K, and the crystal of Compound and shows thermochromism. Compound **8** is a colorless crystal at the room temperature, but at 413 K, it changes their color to red reversibly.

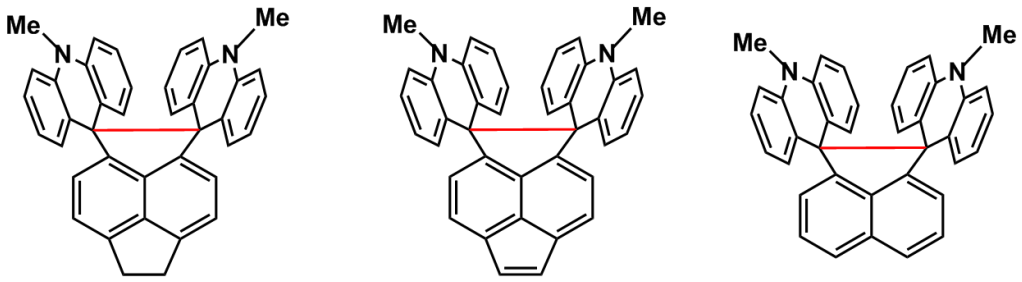

8 **9** **10**

Scheme 5. The structures of Compounds **8**-**10**. The definitions of the "ultralong" C–C length, R_{C-C}, and distortion angle, θ, which are discussed hereafter, are also depicted for Compound **8**.

Table 1. Reported C–C bond length between two acridan rings ($R_{C–C}$) and the distortion angle (θ) of Compound **8**.

Temperature	Label	$R_{C–C}$ [Å]	θ [°]
93 K[12]	Eclipsed 1	1.771(3)	−3.4
	Eclipsed 2	1.758(3)	9.4
	Twisted 1	1.712(2)	23.4
	Twisted 2	1.707(2)	24.7
413 K[13]	Eclipsed	1.791	3.8
	Twisted	1.718	23.7

3.1.4 Extension of the Ultralong C–C Bond at High Temperature

Compound **8** having a long C–C bond was found by X-ray crystal structure analysis to have the existence of a C–C single bond ($R_{C–C}$) with a length of 1.771 Å at 93 K (–180 °C) was confirmed. The researchers reported that $R_{C–C}$ also stretches as the temperature rises when performing a higher temperature X-ray crystal structure analysis. They found that it extends to 1.791 Å at 413 K (140 °C)[11, 13]. In addition, as the temperature of this compound **8** increases, the phase transition of the crystal occurred at 233 K (–40 °C)[11], and the color tone change of the crystal is also confirmed. It has become clear that it shows thermochromism.

3.1.5 Previous Research and Considering Factors

Kawai, Suzuki, and coworkers have reported the synthesis of Compound **8**, a dispirobis(10-methylacridan) derivative, having a ultralong C–C bond between two acridan rings with 1.771 Å at maximum, which was observed by the X-ray experiment at 93 K, where the 4 independent molecules exist in the minimum unit cell[11-13]. The length is clearly longer than the limit of C–C single-bond length proposed by Zavitsas. They also carried out a DFT (density functional theory) geometry optimization for an individual molecule with the B3LYP functional[14], exhibiting the C–C bond length ($R_{C–C}$) of 1.772 Å. However, their calculation did not consider the dispersion interaction, while the intramolecular π–π interaction between two acridan rings facing each other is expected. In addition, the intermolecular interactions, or the environmental effect, are also expected to be important. Table 1 gives $R_{C–C}$ and the distortion angle (θ) of four independent molecules in the crystal structure of Compound **8**. The molecules can be roughly classified into eclipsed and twisted ones, where the absolute value of the distortion angle (θ) are < 10° and > 20°, respectively. $R_{C–C}$, ranging from 1.707 Å to 1.771 Å at 93 K, strongly depends on the environment in the crystal; especially, the eclipsed molecules have relatively longer $R_{C–C}$ than the twisted ones. This tendency can also be seen at 413 K, where the minimum unit cell contains two independent molecules. In this paper, I computationally investigate the sensitivity of this ultralong C–C bond of Compound **8** and its derivatives (Compounds **9** and **10**) focusing on the intramolecular dispersion and intermolecular effects.

3.2 Purposes

Various researches have been done to analyze such long C–C single bonds, but the research done using theoretical calculations can be roughly divided into the following two types. One is to explore the limit of single bond length. The researches on the limit of single bond are considered by Zavitsas[4] and Lee • Nakai[1b], but I have not found that they have investigated the phenomenon where a long C–C bond is maintained. The other is to investigate disconnection of bonds, and such researches have been conducted by Schreiner[15] and Cremer[16]. However, there is no mention about phenomenon in which the state of binding is maintained. Therefore, there are few cases where the state where an ultralong single bond in a compound is maintained is clarified by theoretical calculation, and particularly, no investigation including a peripheral structure has been made with respect to C–C single bond exceeding 1.7 Å. These results would link to the theoretical application to the properties of such compounds.

3.3 Computational Details

3.3.1 Calculations of Monomers

First, I investigated the dispersion effect for the calculation of individual molecule. Here, I carried out the geometry optimization calculations with Gaussian09 program[17]. I adopted cc-pVDZ basis set[18] with BLYP[19], PBEPBE[20], B3LYP[14], BHandHLYP[21], M06-2X[22], CAM-B3LYP[23], and LC-BLYP[19, 24]. I also adopted the wavefunction-based Hartree-Fock (HF) and the second-order Møller-Plesset perturbation (MP2) methods. For PBEPBE and B3LYP functionals, the dispersion interaction is directly taken into account by the D3 correction of Grimme[25], while the M06-2X is known to contain the dispersion effect inside the parametrization.

3.3.2 Calculations of Crystal Structures

To investigate the intermolecular effects for the structures of Compounds **8**–**10**, I next performed the geometry optimization under the periodic boundary condition (PBC). All PBC calculations were carried out with SIESTA program[26] with PBE functional and the double-zeta plus polarization (DZP) basis set. The mesh cutoff energy was set to 200 Ryd. For considering the dispersion interaction, the D2 correction of Grimme[27] was adopted, where the global parameters were set to d = 20.0 and s_6 = 0.75 according to Ref. [27]. The initial geometries were taken from the X-ray structures reported in Ref. [12].

3.3.3 BOMD Calculations

When performing Born-Oppenheimer Molecular Dynamics (BOMD) for Compound **8**, I used GAMESS[28] to investigate the vibration of the coupling corresponding to $R_{C–C}$

over 2000 fs, using PM3. The target structure was based on the structure obtained by monomer optimization (B3LYP).

3.4 Results and Discussions

3.4.1 Calculations of Monomers and the Role of Dispersion

Table 2 shows the functional dependence of $R_{C–C}$ and θ. For PBEPBE and B3LYP functionals, the D3 correction makes $R_{C–C}$ shorter, as is expected by the intramolecular π–π interaction. The difference of $R_{C–C}$ between D3-corrected and uncorrected calculations is 0.022 Å at maximum. According to the shortening of $R_{C–C}$, the distortion angle slightly increases. M06-2X considerably underestimates $R_{C–C}$ and the distortion angle θ increases. I confirm that the intramolecular dispersion interaction moderately affects the ultralong C–C bond lengths. The HF method also considerably underestimates $R_{C–C}$ and interestingly the MP2 elongates $R_{C–C}$ to some extent, while the MP2 method can take the dispersion interaction into account. This can simply be interpreted by recalling the fact that the HF method usually estimates covalent bond stronger. In addition, BHandHLYP underestimates $R_{C–C}$ and the distortion angle θ increases like M06-2X. When the HF exchange ratio of the functional is higher, the calculation estimates shorter $R_{C–C}$. Moreover, when using the functionals with corrections (CAM-B3LYP, LC-BLYP), optimizations underestimate $R_{C–C}$ strongly.

As a supplement, I performed the calculation under UDFT condition (UB3LYP/cc-pVDZ), and the result was same as that under RDFT condition. Therefore, no symmetry-broken solutions were obtained around the crystal structure of Compounds **8**–**10**.

For further understanding the dispersion effect on the structure, the partial geometry optimization calculations with the PBEPBE and PBEPBE-D3 functionals were carried out for Compound **8** with several fixed distortion angles θ. Figure 1 shows the relaxed potential energy curves against the distortion angle. To clearly confirm the dispersion effect, I show the distance between two N atoms in the acridan rings (R_{N---N}) in the Figure

1 together with $R_{C–C}$. Interestingly, for the fixed distortion angle, D3 dispersion correction hardly affect $R_{C–C}$, while it shortens $R_{N\cdots N}$ by more than 0.1 Å. Instead, it deepens the potential energy against the distortion angle and makes the minimum at slightly larger θ. Because $R_{C–C}$ shows negative linear correlation against θ, the D3 correction makes $R_{C–C}$ shorter in the fully relaxed calculation. In any case, the dispersion interaction is important for the structures of these compounds.

Table 2. Comparison of the C–C bond length between two acridan rings ($R_{C–C}$, in Å) and the distortion angle (θ, in °) of Compounds calculated for isolated molecule by DFT, HF, and MP2 methods.

	Compound **8**		Compound **9**		Compound **10**	
Method	$R_{C–C}$	θ	$R_{C–C}$	θ	$R_{C–C}$	θ
BLYP	2.758	0.0	2.788	4.2	2.496	2.6
PBEPBE	1.790	17.7	1.799	17.9	1.723	18.8
PBEPBE-D3	1.779	19.3	1.789	19.4	1.717	20.1
B3LYP	1.772	16.3	1.780	16.4	1.717	17.7
B3LYP-D3	1.750	19.5	1.758	19.5	1.701	20.2
UB3LYP	1.772	16.3	1.780	16.4	1.717	17.7
BHandHLYP	1.707	18.5	1.712	18.3	1.672	19.2
M06-2X	1.704	20.5	1.708	20.4	1.669	21.1
CAM-B3LYP	1.708	18.5	1.712	18.4	1.673	19.2
LC-BLYP	1.662	20.2	1.665	20.0	1.636	20.7
HF	1.693	19.1	1.697	18.9	1.664	19.8
MP2	1.709	21.5	1.715	21.6	1.670	22.0

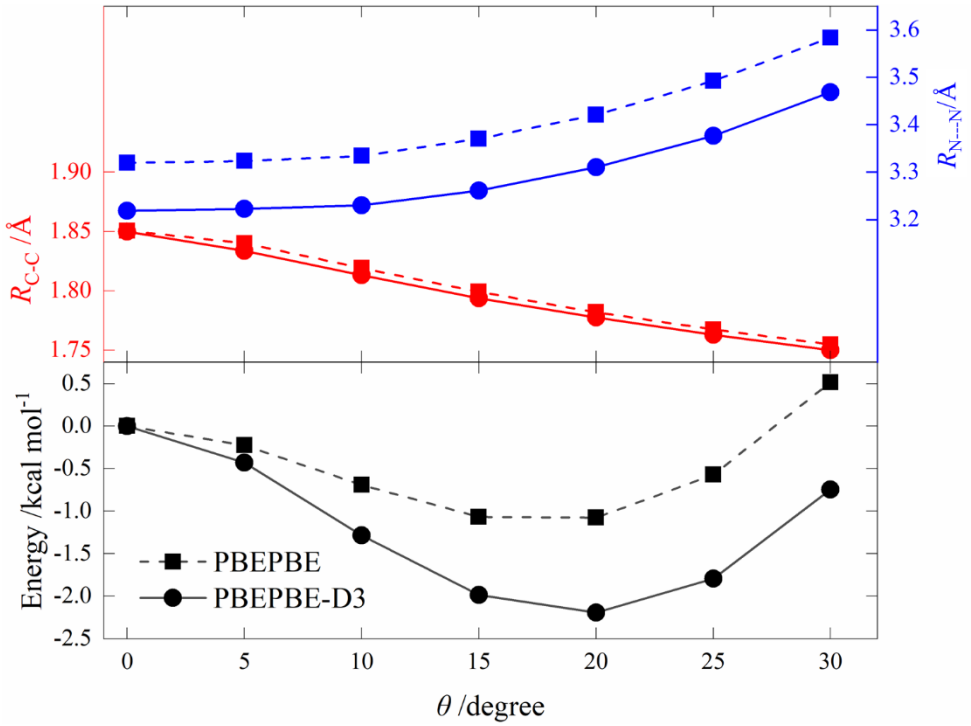

Figure 1. Distortion angle (θ) dependence of the potential energy (in black), $R_{C–C}$ (in red), and $R_{N\cdots N}$ (in blue) obtained by the PBEPBE(-D3) partial geometry optimization calculations of Compound **8**.

In addition, I investigated the existence of the ultralong C–C bond. Figure 2 shows the HOMO orbital of the Compound **8** (PBEPBE-D3). Between carbon atoms, which form the ultralong C–C single bond, there is a bonding σ orbital. When using other functionals, I obtained the same HOMO orbitals as the orbital for PBEPBE-D3. Therefore, we can check the existence of the ultralong C–C bond visually. Table 3 shows the Bond Critical Point ρ and $\nabla^2\rho$ of the Compounds **8-10**, ethane, and ethane whose C–C bond is fixed at 1.750 Å. Such values were obtained with NBO 6.0 program[29]. Comparing the 1.750 Å of ethane, Compound **8** (DSAP), and the derivatives (Compound **9**, **10**) have the ultralong C–C bonds.

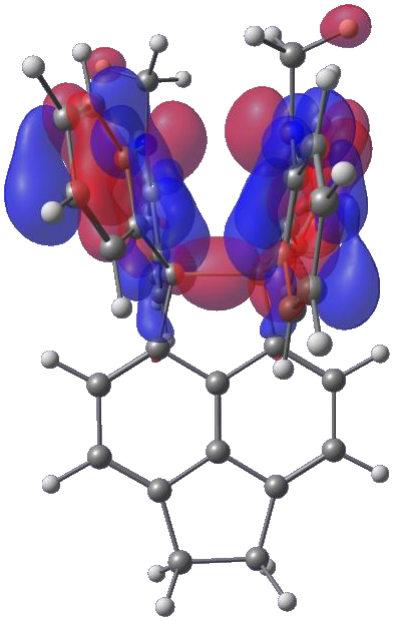

Figure 2. The HOMO of the Compound **8**. There is a bonding σ orbital between the C atoms which form the ultralong C–C bond (R_{C-C}).

Table 3. Indicators regarding the ultralong C–C bonds of Compounds 4–6, obtained from the PBEPBE-D3/cc-pVDZ results with NBO 6.0 program[29].

Compound	$R_{C–C}$	Wiberg [a]	NLMO/NPA-BO [b]	BCP ρ [c]	BCP $\nabla^2\rho$ [d]
Compound **8**	1.779	0.7736	0.8854	0.1507	−0.1979
Compound **9**	1.789	0.7653	0.8810	0.1480	−0.1899
Compound **10**	1.717	0.8096	0.9060	0.1691	−0.2492
Ethane	1.530	1.0552	1.0256	0.2357	−0.4807
Ethane [e]	1.750 [e]	1.0207	1.0101	0.1585	−0.2436

a) Wiberg bond index in natural atomic orbital basis.

b) Natural localized molecular orbital (NLMO)/natural population analysis (NPA) bond order.

c) Electron density at bond critical point.

d) Laplacian of electron density at bond critical point.

e) Ethane molecule with fixed C–C bond length at 1.750 Å.

3.4.2 Calculations of Crystal Structures

Table 4 summarizes the $R_{C–C}$ and θ of Compounds **8**–**10** obtained by the PBC calculations and X-ray experiments. By considering the surrounding molecules, computationally obtained structures of four molecules in the unit cell of Compound **8** can roughly be classified into the eclipsed ones with longer $R_{C–C}$ and twisted ones with shorter $R_{C–C}$, as like the X-ray structure. Comparing with the results shown in Table 4, $R_{C–C}$ of the twisted molecules are considerably shortened, while those of the eclipsed ones are slightly changed. Even without the dispersion correction, the difference between the longest and the shortest $R_{C–C}$ is 0.062 Å, which is in good agreement with the experimental value of 0.064 Å, although the obtained lengths are systematically ~0.03 Å longer than the experiment. The distortion angle θ also shows good agreement within 2°. Similar tendency can also be confirmed for Compound **9**, where the minimum unit cell contains 1 eclipsed and 2 twisted molecules. Considering the dispersion interaction makes $R_{C–C}$ slightly shorter, as was seen for the isolated molecule. The cell volumes of Compounds **8**–**10** by PBC calculations and X-ray experiments are summarized in Table 5. The dispersion correction clearly compensates the overestimation of the cell volume. In addition, comparing the calculated $R_{N\cdots N}$ with experimental ones which are summarized in Table 6, it can also be confirmed that the dispersion corrected results show better agreement of $R_{N\cdots N}$ than the uncorrected ones. These findings suggest that the intermolecular dispersion interaction, as well as the intramolecular one, plays an important role for the crystal structure of these compounds.

I also performed the SIESTA PBE/DZP geometry optimization calculations for isolated molecules with sufficiently large unit cell (a cube of side 20 Å) and compared the results with Gaussian PBEPBE/cc-pVDZ ones. The results of $R_{C–C}$ and θ are shown in Table 7.

Although the SIESTA calculations give shorter $R_{C–C}$ and larger θ than Gaussian ones do, it could be confirmed that the tendency of the structure is similar.

In addition, the attention is paid to the influence of dispersion. Comparing the difference from the results of optimization of the crystal structure of Compound **8**, the value change of the distortion angles (θ) are different from the Eclipsed molecules and the Twisted molecules. The calculations of monomers are performed in the unit cell with the fixed distortion angle, θ (PBEPBE(-D3)/cc-pVDZ). The results of $R_{C–C}$ were shown in Table 7, all the molecules underestimate *R*c-c under introducing dispersion. When comparing the energies, the Twisted molecules were more stable. As a result, the environmental effects are more important to $R_{C–C}$, comparing the dispersion.

Table 4. C–C bond length between two acridan rings ($R_{C–C}$, in Å) and the distortion angle (θ, in °) of Compound **8-10** calculated for the crystal structure.

	GGA-PBE		GGA-PBE-D2		Exptl.[12, 13]	
Molecule	$R_{C–C}$	θ	$R_{C–C}$	θ	$R_{C–C}$	θ
Compound **8** @93 K						
Eclipsed 1	1.797	−4.2	1.791	–3.5	1.771	−3.4
Eclipsed 2	1.782	10.6	1.771	10.5	1.758	9.4
Twisted 1	1.745	21.7	1.705	25.5	1.712	23.4
Twisted 2	1.735	23.3	1.717	24.3	1.707	24.7
Compound **8** @413 K						
Eclipsed	1.781	10.0	1.800	3.1	1.791	3.8
Twisted	1.749	20.9	1.711	24.8	1.718	23.7
Compound **9**						
Eclipsed	1.788	6.1	1.753	6.6	1.749	5.5
Twisted 1	1.745	22.1	1.721	23.8	1.726	21.3
Twisted 2	1.752	21.3	1.716	24.2	1.721	22.8
Compound **10**						
(no label)	1.703	18.3	1.684	18.6	1.696	18.1

Table 5. Cell volumes (in Å^3) of Compounds **8-10** obtained by the PBC calculations and X-ray experiments.

Molecule	GGA-PBE	GGA-PBE-D2	Exptl.[12]
Compound **8** @93 K	6416	5130	5439
Compound **8** @413 K	3250	2569	2823
Compound **9**	5207	4167	4501
Compound **10**	3030	2440	2601

Table 6. Comparison of the distance between two N atoms ($R_{N...N}$, in Å) of Compound **8**.

		PBE	PBE-D2	Exptl.
Isolated molecule		3.395 [a)]	3.303 [b)]	
Crystal structure	Eclipsed 1	3.359	3.161	3.200
	Eclipsed 2	3.374	3.154	3.192
	Twisted 1	3.453	3.276	3.299
	Twisted 2	3.402	3.284	3.307

[a)] Gaussian PBEPBE/cc-pVDZ result

[b)] Gaussian PBEPBE-D3/cc-pVDZ result

Table 7. C–C bond length between two acridan rings ($R_{C–C}$, in Å) and the distortion angle (θ, in °) of Compound **8**-**10** calculated for monomer with periodical boundary condition (in a 20×20×20 cell).

	GGA-PBE		GGA-PBE-D2	
Molecule	$R_{C–C}$	θ	$R_{C–C}$	θ
Compound **8**	1.754	18.4	1.722	22.8
Compound **9**	1.757	18.7	1.728	22.7
Compound **10**	1.703	19.1	1.687	21.1

3.4.3 BOMD Calculation to investigate the stretch of C–C bond

First, I picked up four C–C single bonds in Compound **8** and classified into four colors of red, blue, green, and pink in Figure 3. For the four bonds, I examined how the bond expansion and contraction is schematically changed by changing the temperature condition (93 K and 413 K). Table 8 and 9 show the average of each C–C bond length in BOMD at 2000 fs (Table 7 shows 93 results). The difference in length was 0.02 Å, which was a large value compared with the fact that the other green, blue and pink C–C bonds were not transformed at 0.001 Å. I found that the elongation accompanied with the temperature rise and the elongation margin was larger than those of the other single bonds. I carried out the BOMD calculation as a monomer, but the extension within the crystal structure is a situation where the surrounding structure exists. It is possible to explain the phenomenon that the long single bond extends compared to other bonds.

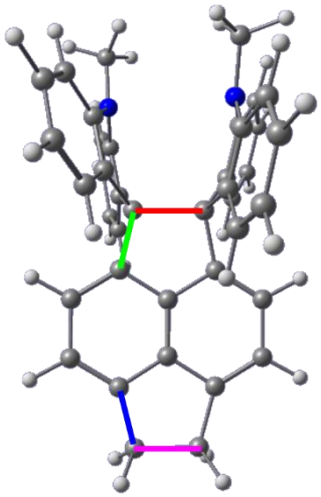

Figure 3. The object of the four kinds of C–C bonds (including R_{C-C}) in four colors (red, green, blue, pink). R_{C-C} is described in red.

Table 8. The average length of four C–C bonds through the BOMD calculation (93 K, 2000fs).

	R_{C-C} (Red)	C–C (Green)	C–C (Blue)	C–C (Pink)
93 K	1.694	1.526	1.503	1.571

Table 9. The average length of four C–C bonds through the BOMD calculation (413 K, 2000fs).

	R_{C-C} (Red)	C–C (Green)	C–C (Blue)	C–C (Pink)
413 K	1.712	1.530	1.507	1.572

3.5 Conclusion

In conclusion, I confirmed that the intramolecular and intermolecular dispersion interactions as well as the crystal packing effect cooperatively realize the ultralong C–C single bond of Compound **8**. In addition, BOMD analysis of Compound **8** has revealed that it is possible theoretically. Moreover, I have published the paper about calculation considering the dispersion and crystal structures[30].

Recently, Ishigaki *et al*. synthesized the compound where the acridan rings of Compound **9** are substituted with dibenzocycloheptatriene rings and reported that the molecule has a C–C single bond over 1.8 Å length[31]. Theoretical investigation on the hyper covalent bond of this molecule is shown in Chapter 4.

3.6 References

1. a) P. R. Schreiner, L. V. Chernish, P. A. Gunchenko, E. Yu. Tikhonchuk, H. Hausmann, M. Serafin, S. Schlecht, J. E. P. Dahl, R. M.K. Carlson, A. A. Fokin, *Nature*, **2011**, *477*, 308; b) D. Cho, Y. Ikabata, T. Yoshikawa, J. Y. Lee, H. Nakai, *Bull. Chem. Soc. Jpn.* **2015**, *88*, 1636.
2. F. Toda, K. Tanaka, M. Watanabe, K. Tamura, I. Miyahara, T. Nakai, K. Hirotsu, *J. Org. Chem.* **1999**, *64*, 3102.
3. J. L. Adcock, A. A. Gakh, J. L. Pollitte, C. Woods, *J. Am. Chem. Soc.* **1992**, *114*, 3980.
4. A. A. Zavitsas, *J. Phys. Chem. A* **2003**, *107*, 897.
5. L. Pauling, The Nature of the Chemical Bond and the Structure of Molecules and Crystal: An Introduction to Modern Structural Chemistry, Cornell University Press, Ithaca, NY, 3rd edn., **1960**.
6. T. Takeda, Y. Uchimura, H. Kawai, R. Katoono, K. Fujiwara, T. Suzuki, *Chem. Commun.* **2014**, *50*, 3924.
7. M. Tanaka, A. Sekiguchi, *Angew. Chem. Int. Ed.* **2005**, *44*, 5821.
8. J. M. McBride, *Tetrahedron*, **1974**, *30*, 2009.
9. G. Wittig, H. Petri, *Liebigs Ann. Chem.* **1933**, *505*, 17.
10. To pick up the similar case, T. Nishiuchi, S.-y. Uno, Y. Hirao, T. Kubo. *J. Org. Chem.* **2016**, *81*, 2106.
11. H. Kawai, T. Takeda, K. Fujiwara, T. Inabe, T. Suzuki, *Crys. Growth Des.* **2005**, *5*, 2256.
12. H. Kawai, T. Takeda, K. Fujiwara, M. Wakeshima, Y. Hinatsu, T. Suzuki, *Chem. Eur. J.* **2008**, *14*, 5780.

13. T. Takeda, H. Kawai, R. Herges, E. Mucke, Y. Sawai, K. Murakoshi, K. Fujiwara, T. Suzuki, *Tetrahedron Lett.* **2009**, *50*, 3693.
14. a) A. D. Becke, *J. Chem. Phys.* **1993**, *98*, 5648; b) P. J. Stephens, F. J. Devlin, C. F. Chabalowski, M. J. Frisch, *J. Phys. Chem.* **1994**, *98*, 11623.
15. S. Rösel, C. Balestrieri, P. R. Schreiner, *Chem. Sci.* **2017**, *8*, 405.
16. A. Humason, W. Zou, D. Cremer, *J. Phys. Chem. A* **2015**, *119*, 1666.
17. M. J. Frisch, G. W. Trucks, H. B. Schlegel, G. E. Scuseria, M. A. Robb, J. R. Cheeseman, G. Scalmani, V. Barone, B. Mennucci, G. A. Petersson, H. Nakatsuji, M. Caricato, X. Li, H. P. Hratchian, A. F. Izmaylov, J. Bloino, G. Zheng, J. L. Sonnenberg, M. Hada, M. Ehara, K. Toyota, R. Fukuda, J. Hasegawa, M. Ishida, T. Nakajima, Y. Honda, O. Kitao, H. Nakai, T. Vreven, J. A. Montgomery, Jr., J. E. Peralta, F. Ogliaro, M. Bearpark, J. J. Heyd, E. Brothers, K. N. Kudin, V. N. Staroverov, T. Keith, R. Kobayashi, J. Normand, K. Raghavachari, A. Rendell, J. C. Burant, S. S. Iyengar, J. Tomasi, M. Cossi, N. Rega, J. M. Millam, M. Klene, J. E. Knox, J. B. Cross, V. Bakken, C. Adamo, J. Jaramillo, R. Gomperts, R. E. Stratmann, O. Yazyev, A. J. Austin, R. Cammi, C. Pomelli, J. W. Ochterski, R. L. Martin, K. Morokuma, V. G. Zakrzewski, G. A. Voth, P. Salvador, J. J. Dannenberg, S. Dapprich, A. D. Daniels, O. Farkas, J. B. Foresman, J. V. Ortiz, J. Cioslowski, D. J. Fox, Gaussian09 (Revision D.01), Gaussian, Inc., Wallingford, CT, **2013**.
18. T. H. Dunning, Jr., *J. Chem. Phys.* **1989**, *90*, 1007.
19. A. D. Becke, *Phys. Rev. A.* **1988**, *38*, 3098.
20. a) J. P. Perdew, K. Burke, M. Ernzerhof, *Phys. Rev. Lett.* **1996**, *77*, 3865. b) J. P. Perdew, K. Burke, M. Ernzerhof, *Phys. Rev. Lett.* **1997**, *78*, 1396.
21. A. D. Becke, *J. Chem. Phys.* **1993**, *98*, 1372.

22. Y. Zhao, D. G. Truhlar, *Theor. Chem. Acc.* **2008**, *120*, 215.

23. T. Yanai, D. P. Tew, N. C. Handy, *Chem. Phys. Lett.* **2004**, *91*, 51.

24. H. Iikura, T. Tsuneda, T. Yanai, K. Hirao, *J. Chem. Phys.* **2001**, *115*, 3540.

25. S. Grimme, J. Antony, S. Ehrlich, H. Krieg, *J. Chem. Phys*. **2010**, *132*, 154104.

26. a) J. J. P. Stewart, *J. Mol. Model.* **2007**, *13*, 1173.; b) J. M. Soler, E. Artacho, J. D. Gale, A. García, J. Junquera, P. Ordejón, D. Sánchez-Portal, *J. Phys.: Cond. Matt.* **2002**, *14*, 2745.

27. S. Grimme, *J. Comput. Chem.* **2006**, *27*, 1787.

28. Y. Zhao, D. G. Truhlar, *Theor. Chem. Acc.* **2008**, *120*, 215. a) M. W. Schmidt, K. K. Baldridge, J. A. Boatz, S. T. Elbert, M. S. Gordon, J. H. Jensen, S. Koseki, N. Matsunaga, K. A. Nguyen, S. Su, T. L. Windus, M. Dupuis, J. A. Montgomery, *J. Comput. Chem.* **1993**, *14*, 1347; b) M. S. Gordon, M. W. Schmidt, in "Theory and Applications of Computational Chemistry: the first forty years" ed. by C. E. Dykstra, G. Frenking, K. S. Kim, G. E. Scuseria, Elsevier, Amsterdam, **2005**, pp. 1167-1189.

29. E. D. Glendening, J. K. Badenhoop, A. E. Reed, J. E. Carpenter, J. A. Bohmann, C. M. Morales, C. R. Landis, F. Weinhold, NBO 6.0, University of Wisconsin, Madison, WI, **2013**; http://nbo6.chem.wisc.edu/.

30. Y. Kuroda, M. Kobayashi, T. Taketsugu, *Chem. Lett*. *in press.*

31. Y. Ishigaki, T. Shimajiri, T. Takeda, R. Katoono, and T. Suzuki, *Chem*, **2018**, *4*, 795.

4 The Phenomena of the Compound with the C–C Bond over 1.8 Å

4.1 Compound with the C–C Bond over 1.8 Å

In Chapter 3, Two themes were mentioned; (1) the environmental effect of DSAP (Compound **8** in the previous chapter) having a very long C–C bond exceeding 1.7 Å; (2) an ultralong C–C bond extension at a high temperature. In this chapter, Compound **1** (see Scheme 1), are referred to, which has a similar backbone and has a single bond length longer than DSAP.

In 2018, Compound **1** was synthesized by Ishigaki *et al.*[1] According to the results of X-ray crystal structure analysis reported at the same time, $R_{C–C}$ of Compound **1** showed 1.980(18) Å for analysis at 200 K and 1.80(2) Å for 400 K (Table 1). This bond length is longer than the $R_{C–C}$ result of DSAP (See Chapter 3), and there is no other example having a bond exceeding 1.80 Å. Ishigaki calls such a bond a hyper covalent bond. Moreover, the distance between C---C in the non-bond state is 1.80 Å at the shortest, and the length of 1.80 Å corresponds to the boundary between the existence and absence of bonds[2].

The design guideline for Compound **1** is based on the structure of DSAP. The ultralong C–C single bond of DSAP is present in a part surrounded by a rigid framework made of C_{sp2} carbon such as acridan ring. This plays an important role in maintaining the bonding state of weak bond, ultralong C–C single bond without causing diradical formation and isomerization. Ishigaki and co-workers call it "core-shell" strategy[1]. "shell" here refers to a rigid π skeleton like DSAP or Compound **1**. In addition, in Compound **1**, adopting a policy to further elongate weak bonds by distorting the rigid π skeleton[3].

For Compound **1**, various results and insights has been obtained by experiments. According to the report of Ishigaki *et al.*, they suggest that the existence of the bond corresponding to $R_{C–C}$ was convinced by electron density map (*D* map), Raman measurement, and VT-NMR performed at 200 K and 400 K[1]. In addition, for ^{1}HNMR in a solvent (in $CDCl_3$), no significant difference was observed in the immediate analysis result after synthesis and that of the solution left 100 days after immediate NMR analysis after synthesis, including the shape of the peak. Thus, Compound **1** is considered to be maintained stably[1]. Furthermore, from the NMR results of the compound **1**, the symmetry of the molecule could be thought to be C_{2v}, whereas the symmetry from the structure obtained in the crystal structure, C_s was suggested. From these results, it can be pointed out that Compound **1** can perform the flip of two dibenzocycloheptatriene rings as shown in Scheme 2 in solution.

In addition, they have found that this bond cleaves the bond and become dication with oxidation (electron donation)[4]. The dication also returns to the original compound **1** by reduction. Therefore, this redox reaction occurs reversibly and has been confirmed also in cyclic voltammetry (CV). According to the result of CV, they confirmed from the peak that Compound **1** was two-electron oxidized and reduced, but a shoulder exists midway in either the oxidized wave or the reduced wave. This result indicates that the cleavage of very long C–C single bond is going through cation radicals on the way, but on the experiment side the real image has not been captured. At that moment, there are several candidate structures (see Scheme 3) for the cation radical $\mathbf{1}^{+\bullet}$.

Ishigaki and co-workers also measured UV-Vis spectra for the oxidation of Compound **1**[4]. According to the spectra, the peak in ~530 nm has appeared since the oxidation, and the peak of 290 nm has sharpened and then the peak of 300-310 nm sharpened while the

change from $\mathbf{1}^{+\bullet}$ to $\mathbf{1}^{2+}$. The growth of the peak of ~530 nm might be related with the appearance of the cation radical. Moreover, the growth of spectrum around 600 nm is revealed while the oxidation from $\mathbf{1}^{+\bullet}$ to $\mathbf{1}^{2+}$. On the other hand, there is no peak around ~530 nm while measuring Compound **1**.

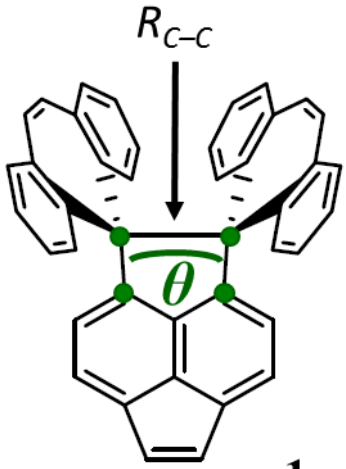

1

Scheme 1. The structure of Compound **1**.

Table 1. Reported C–C bond length between two acridan rings (R_{C-C}) and the distortion angle (θ) of Compound **1**.

Temperature	R_{C-C} [Å]	θ [°]
200 K	1.7980(18)	2.48(10)
400 K	1.806(2)	2.68(12)

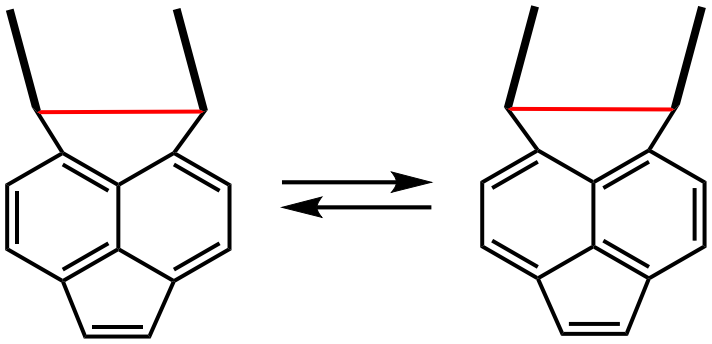

Scheme 2. The possible scheme of the "flip" phenomenon of Compound **1**.

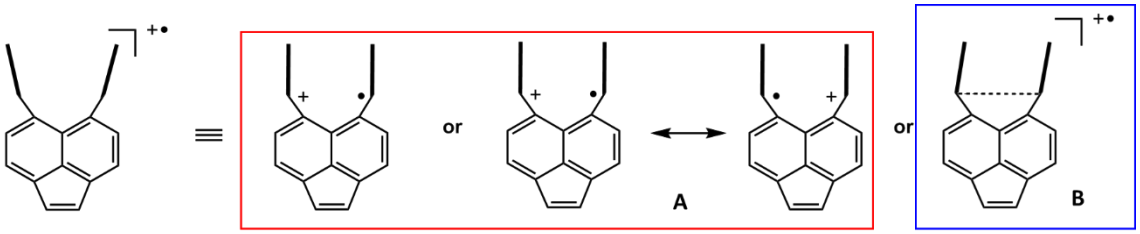

Scheme 3. The imaginable structure of cation radical $\mathbf{1}^{+\bullet}$.

4.2 Purpose

Compound **1** has interesting phenomena which might be related with the “ultralong” C–C bond. Nevertheless, it is very difficult to grasp such phenomena by experimental methods only. The flip occurs in the solution at a low temperature, and there is almost no experimental way to catch up with the movement of dibenzocycloheptatriene rings. In a long run, it would be a clue to analyze the change of property of stimuli-responsive compounds.

4.3 Computational Details

Gaussian16[5] package and DFT calculation (UB3LYP/cc-pVDZ, unless otherwise noted) are applied. In this research, the calculations of cation radical are treated, and UDFT are adopted. For the optimization of Compound **1**, various functionals were used[6-13]. For the calculation on flip, the environment surrounded by the solvent ($CHCl_3$).

4.4 Result and Discussions

4.4.1 Optimization of Monomers

First, the functional dependence of the optimization of Compound **1** monomer was investigated. Table 2 shows the $R_{C–C}$ and distortion angle θ for various functional. The tendency of the dependence for Compound **1** was same as that for DSAP. In addition, UDFT calculations were also performed, and the results were almost same as those of RDFT calculations. And then, no symmetry-broken solutions were obtained around the crystal structure for Compound **1**.

Table 2. Comparison of the C–C bond length between two acridan rings ($R_{C–C}$, in Å) and the distortion angle (θ, in °) of Compounds **1**, which is calculated for isolated molecule by DFT.

Functional	$R_{C–C}$	θ	
BLYP		2.808	0.0
PBEPBE		1.845	0.0
PBEPBE-D3		1.852	0.0
B3LYP		1.836	0.0
B3LYP-D3		1.833	0.0
BHandHLYP		1.766	0.0
M06-2X		1.767	0.0
CAM-B3LYP		1.763	0.0
LC-BLYP		1.713	0.0

4.4.2 Flip Reaction

It is necessary to summarize the mechanism by which flip progresses, suggested to occur in Compound **1**. The functional is fixed with UB3LYP, and the basis function is cc-pVDZ. First, attention was paid to the angle *A* formed by three carbon atoms shown in Figure 1. Calculating what happens to the energy while gradually changing the angle value is shown in Figure 2 in the behavior of flip.

According to Figure 2, I consider that there are two paths of flip from EQ1 confirmed by the original crystal structure to EQ3 showing almost the same stability as EQ1. This pathway is by way of a metastable structure (EQ2 or EQ4, Figure 2) rather than a path which directly connects structures whose dibenzocycloheptatriene ring tilts in one direction. There is one metastable structure in each path, but the difference between the metastable structures is only the plus or minus of the distortion angle is reversed. Among them, Figure 3 shows the energy diagram of the path that reaches EQ3 from EQ1 via EQ2. The zero-point of the relative energy was set as EQ1. The relative energy of transition state TS1 going to EQ2 and transition state TS2 on the way from EQ2 to EQ3 is ca. 0.7 kcal mol^{-1}, which is an energy barrier that can sufficiently overcome even at low temperatures.

Also, the energy diagram of the path from EQ1 to EQ3 via EQ4 is shown in Figure 4. This route is almost the same as the route shown in Figure 3, and it concludes that it passes through either of these paths when flipping.

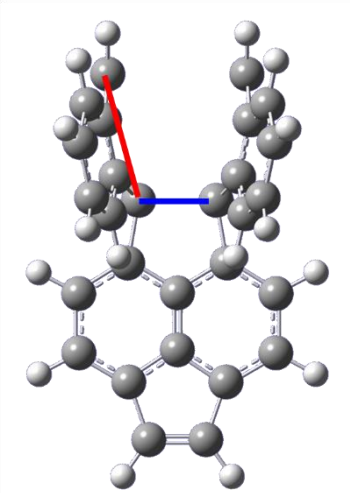

Figure 1. The difinition of A; The angle of the blue line (including R_{C-C}) and the red line (The one C atom which consists of R_{C-C}, and the one C atom)

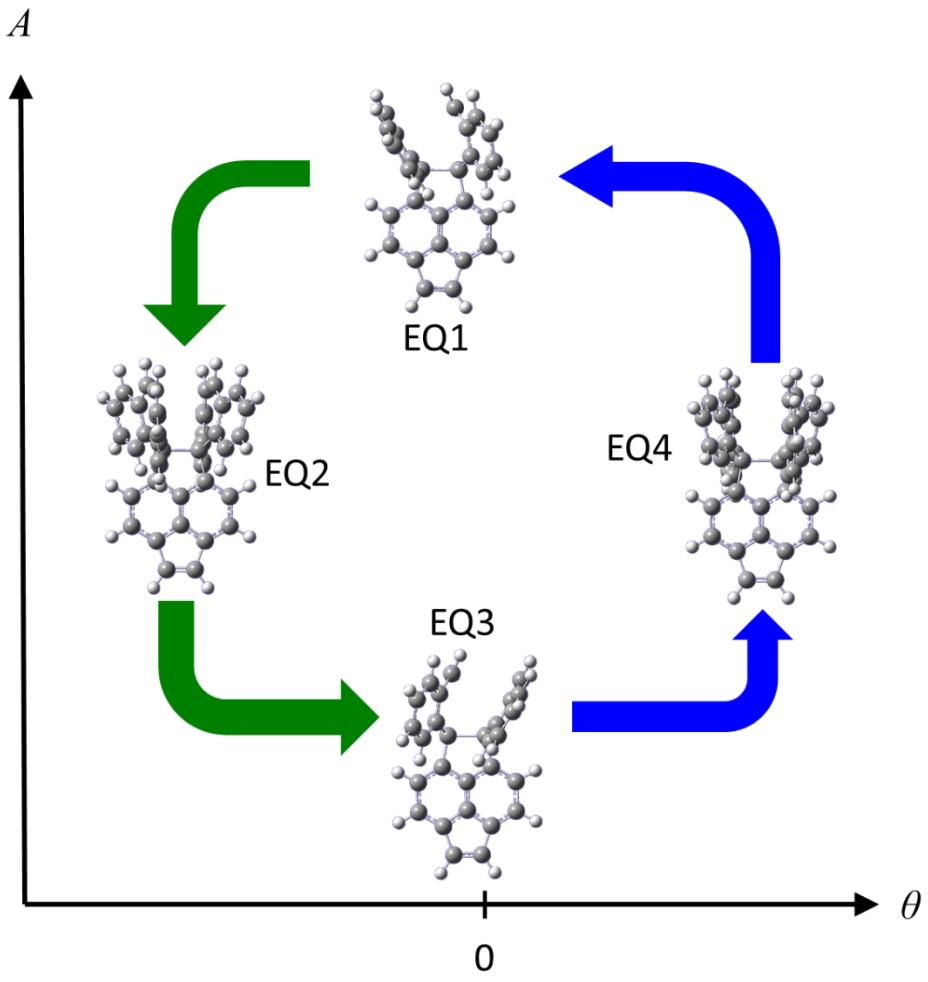

Figure 2. The simple images of the two flipping paths.

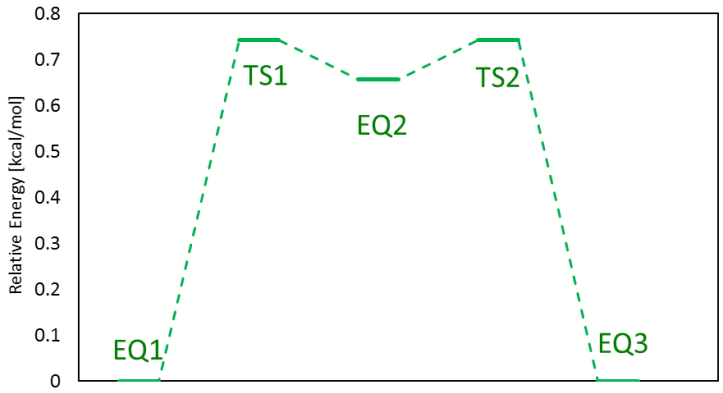

Figure 3. The energy diagram for flip (From EQ1 ~ EQ2 ~ EQ3; The green route in Figure 2).

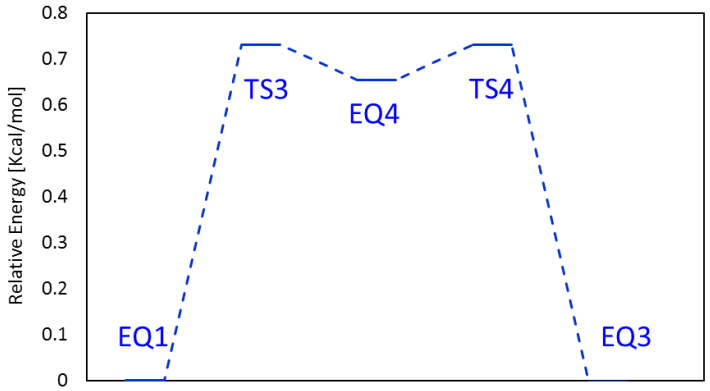

Figure 4. The energy diagram for flip (From EQ1 ~ EQ4 ~ EQ3; The blue route in Figure 2).

Here, in order to confirm the existence of a route approaching directly from EQ1 to EQ3, an energy potential surface around these four stable structures (including the metastable structure) was created. The figure is shown in Figure 5. A secondary saddle point where two of the force constants are imaginary was found at $A = 100$ ° and $\theta = 0$ °. This structure is shown in Figure 6. The energy barrier of the path directly from EQ1 to EQ3 is ca. 1.5 kcal mol^{-1}, but the energy barriers through EQ2 or EQ4 are smaller. The structure of Figure 6 corresponds to the C_{2v} structure proposed by the NMR spectra of Compound **1**, which reflects the three insights: (1) The flip occurs reversibly; (2) There are two paths in flipping and the activation energies in both paths are almost same; (3) the intermediates of both paths are only differs from the plus or minus of distortion angle, θ.

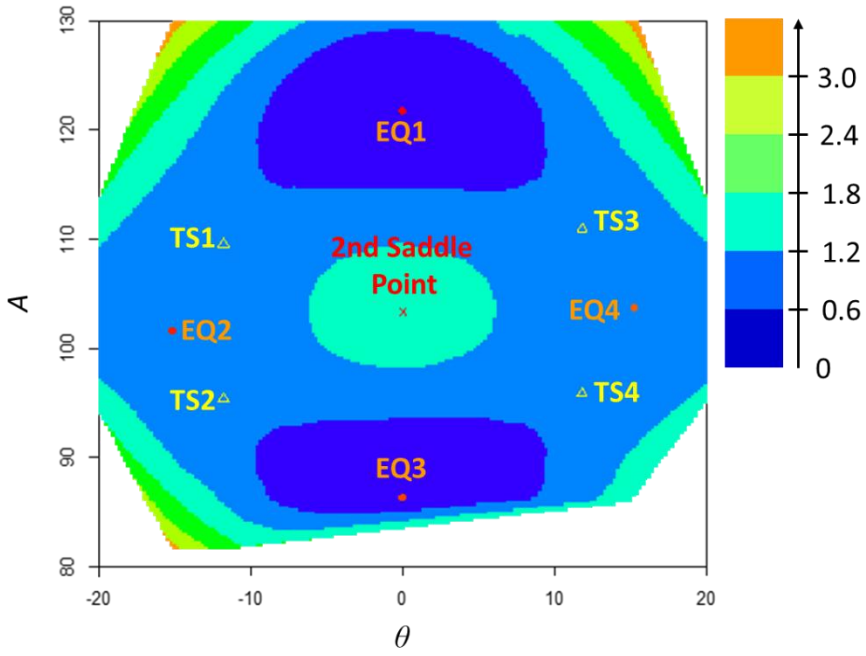

Figure 5. The potential energy surface of "flip"; ●: EQ, △: TS, ×: second saddle point.

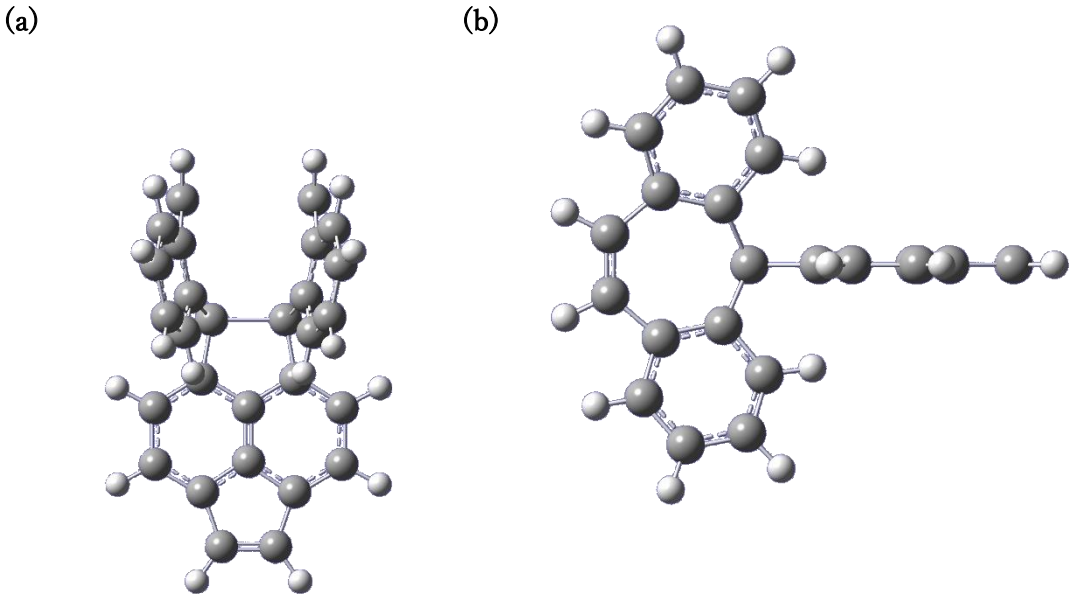

Figure 6. The second-saddle structure of Compound **1**: (a) Front view; (b) Side view.

4.4.3 Cation Radical

According to the result cyclic voltammetry, there is a peak in each shoulder of the oxidation/reduction wave, and I assume that the stepwise oxidation and reduction occur. However, it is difficult to identify the existence of the intermediate (i.e. cation radical). At that moment, two structures are considered; Structure **B** (See Scheme 3), whose ultralong C–C bond completely cleaves, or Structure **A** which maintain the C–C bond, like Compound **1**.

First, I performed the optimizations of structure **A** and **B**. Table 3 shows the $R_{C–C}$ and relative energies, whose benchmark is the total energy of Structure **A**. According Table 3, Structure **B**, whose ultralong C–C bond cleaves is more stable than Structure **A**. Moreover, Figure 7 explains the change of the energies while the $R_{C–C}$ stretches (There is no solvent effects). Thus, these results explain that Structure **B** is stable and the ultralong C–C bond is cleaving when Compound **1** transfers to $\mathbf{1}^{+\bullet}$.

According to the UV-Vis spectra for Compound **1**, I performed TD-DFT calculations (TD-UB3LYP/cc-PVDZ, State = 300). Figure 8 shows the calculated spectra of Compound **1**, $\mathbf{1}^{+\bullet}$, and $\mathbf{1}^{2+}$. The experimental peaks of $\mathbf{1}^{+\bullet}$ and $\mathbf{1}^{2+}$, which appears around 530 nm has shifted to ca. 580 nm and broadened to the higher wave length. The broadening is similar to the experimental report of the transfer from the cation radical to the dication. there is an oscillator (f = 0.0289) at ca. 575 nm for $\mathbf{1}^{2+}$, and this is the π–π* transfer (HOMO–1 → LUMO+1). In the transfer, π orbitals derive from the π skeletons of dibenzocycloheptatriene rings and dihydropyracylene skeleton, and π* orbitals also arise from them.

The comparison of Structure **A** and **B** is also performed. Figure 9 shows the UV-Vis spectra of Structure **A** and **B**. Paying attention to the peak over 500 nm, there is a broad

peak in the spectrum of Structure **A** only. According to the experimental spectrum of Compound $\mathbf{1}^{+\bullet}$ and $\mathbf{1}^{2+}$, there is a peak between 500-600 nm. So, the structure in the sample for UV-Vis spectrum, seems to be close to the Structure **A**.

Table 3. The $R_{C–C}$ and distortion angle θ, and relative energy of Structure **A** and **B**.

Structure	$R_{C–C}$ [Å]	θ [°]	Relative Energy [kcal]
Structure **A**	3.152	23.6	–60.93
Structure **B**	1.810	0.0	0.00

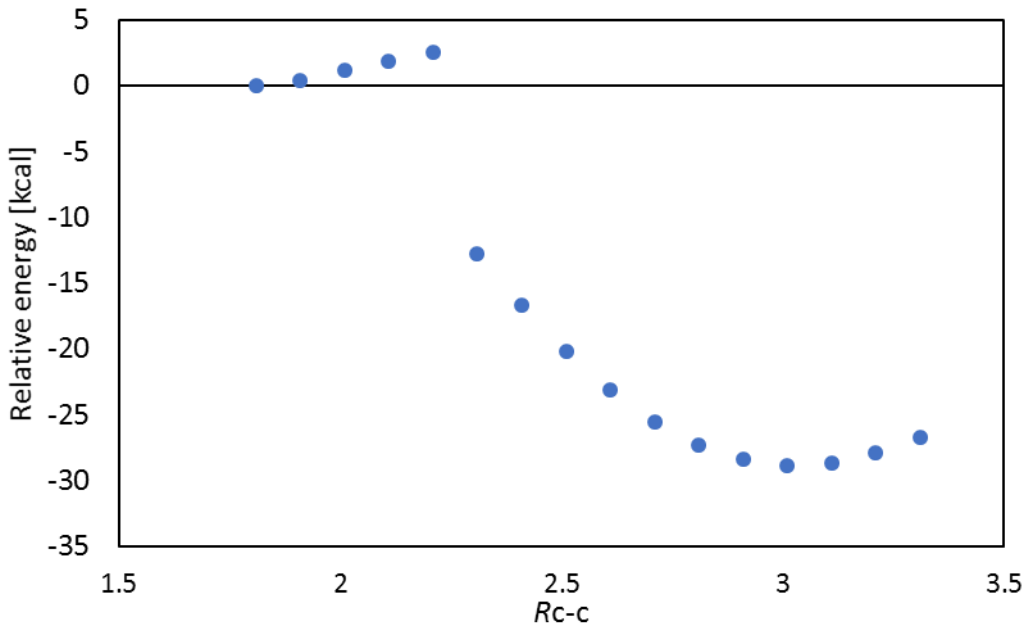

Figure 7. The relationship between the relative energy and $R_{C–C}$.

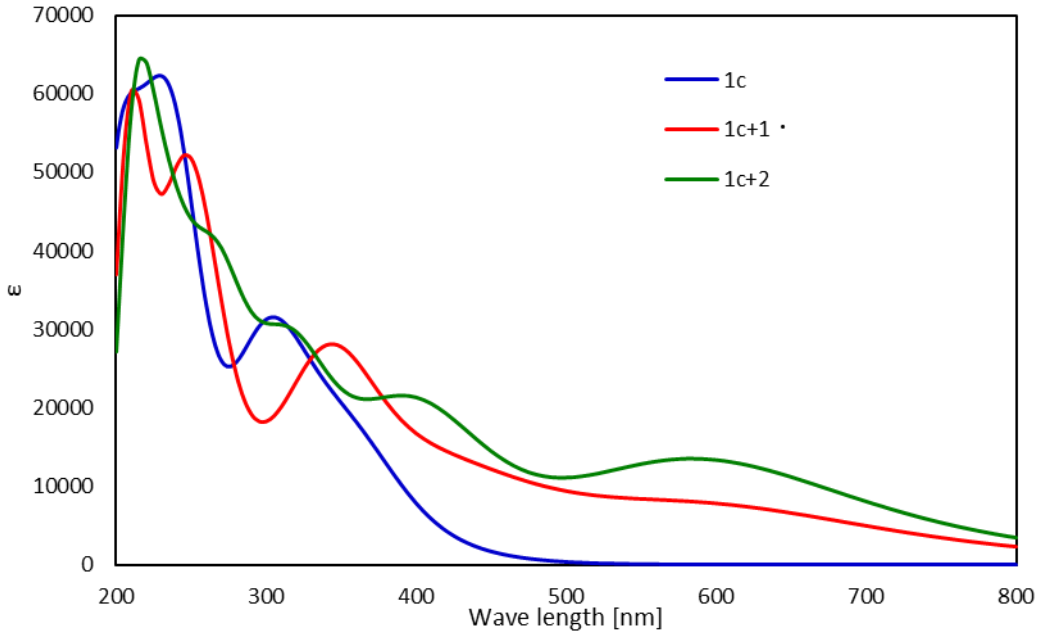

Figure 8. Calculated UV-Vis spectra of Compound **1**, cation radical $\mathbf{1}^{+\bullet}$, and dication $\mathbf{1}^{2+}$.

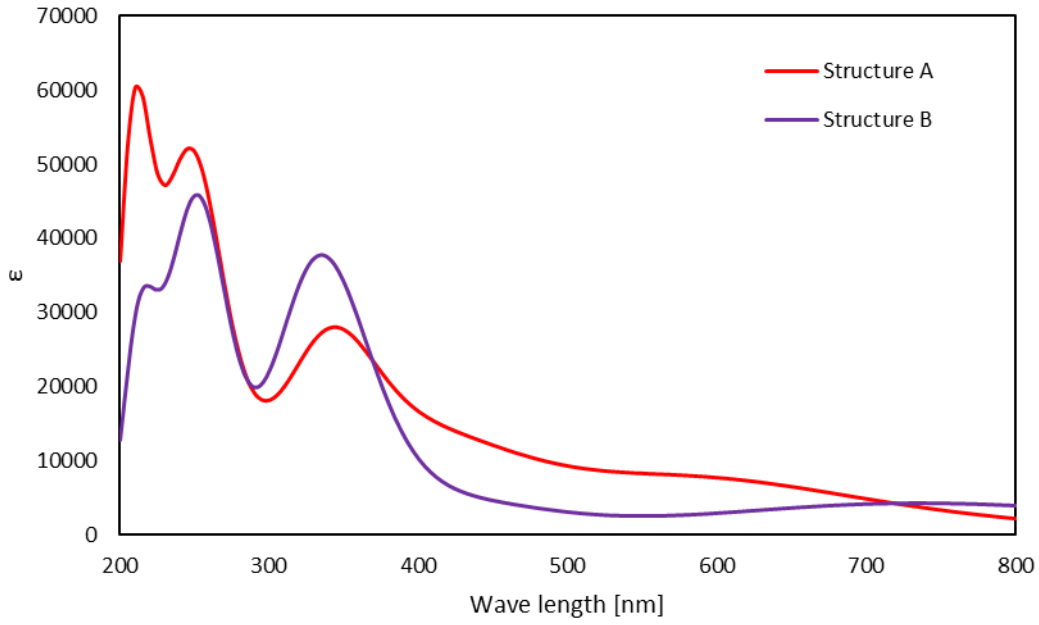

Figure 9. Calculated UV-Vis spectra of Cation radicals ($\mathbf{1}^{+\bullet}$) of Structure **A** and **B**.

4.5 Conclusion

I revealed that the difference of the symmetry of Compound **1** between the structure in the solvent and the crystal structure. In the crystal structure, the symmetry of Compound **1** shows C_s, derives from the most stable structure in energy. On the other hand, the symmetry of Compound **1** in solvent shows C_{2v}, arises from the flipping. In this flip, Compound **1** forms two types of the most stable structure, and the average image is the structure of the second saddle point of flipping.

Then, the image of cation radical is investigated. Comparing the energy, the structure, whose ultralong C–C bond is cleaved, is more stable than that, whose ultralong C–C bond is maintained. The difference of the calculation for the UV-Vis spectra at the peak of 500-600 nm confirms this result.

In this chapter, I investigated the phenomena which are related with the ultralong covalent bond. These researches reported in this chapter would be expected to be linked with the clarification of the change of the properties related with long covalent bonds and the breakthrough to find the “stimuli-responsive” materials.

4.6 References

1. Y. Ishigaki, T. Shimajiri, T. Takeda, R. Katoono, and T. Suzuki, *Chem*, **2018**, *4*, 795.
2. J. L. Adcock, A. A. Gakh, J. L. Pollitte, C. Woods, *J. Am. Chem. Soc.* **1992**, *114*, 3980.
3. Y. Uchimura, T. Takeda, R. Katoono, K. Fujiwara, T. Suzuki, *Angew. Chem. Int. Ed.* **2015**, *54*, 4010.
4. Y. Kuroda, M. Kobayashi, T. Taketsugu, Y. Ishigaki, T. Suzuki, a private talk on March 27.
5. Gaussian 16, Revision B.01, M. J. Frisch, G. W. Trucks, H. B. Schlegel, G. E. Scuseria, M. A. Robb, J. R. Cheeseman, G. Scalmani, V. Barone, G. A. Petersson, H. Nakatsuji, X. Li, M. Caricato, A. V. Marenich, J. Bloino, B. G. Janesko, R. Gomperts, B. Mennucci, H. P. Hratchian, J. V. Ortiz, A. F. Izmaylov, J. L. Sonnenberg, D. Williams-Young, F. Ding, F. Lipparini, F. Egidi, J. Goings, B. Peng, A. Petrone, T. Henderson, D. Ranasinghe, V. G. Zakrzewski, J. Gao, N. Rega, G. Zheng, W. Liang, M. Hada, M. Ehara, K. Toyota, R. Fukuda, J. Hasegawa, M. Ishida, T. Nakajima, Y. Honda, O. Kitao, H. Nakai, T. Vreven, K. Throssell, J. A. Montgomery, Jr., J. E. Peralta, F. Ogliaro, M. J. Bearpark, J. J. Heyd, E. N. Brothers, K. N. Kudin, V. N. Staroverov, T. A. Keith, R. Kobayashi, J. Normand, K. Raghavachari, A. P. Rendell, J. C. Burant, S. S. Iyengar, J. Tomasi, M. Cossi, J. M. Millam, M. Klene, C. Adamo, R. Cammi, J. W. Ochterski, R. L. Martin, K. Morokuma, O. Farkas, J. B. Foresman, and D. J. Fox, Gaussian, Inc., Wallingford CT, **2016**.
6. a) A. D. Becke, *J. Chem. Phys.* **1993**, *98*, 5648; b) P. J. Stephens, F. J. Devlin, C. F. Chabalowski, M. J. Frisch, *J. Phys. Chem.* **1994**, *98*, 11623.
7. A. D. Becke, *Phys. Rev. A.* **1988**, *38*, 3098.
8. a) J. P. Perdew, K. Burke, M. Ernzerhof, *Phys. Rev. Lett.* **1996**, *77*, 3865. b) J. P.

Perdew, K. Burke, M. Ernzerhof, *Phys. Rev. Lett.* **1997**, *78*, 1396.

9. A. D. Becke, *J. Chem. Phys.* **1993**, *98*, 1372.
10. Y. Zhao, D. G. Truhlar, *Theor. Chem. Acc.* **2008**, *120*, 215.
11. T. Yanai, D. P. Tew, N. C. Handy, *Chem. Phys. Lett.* **2004**, *91*, 51.
12. H. Iikura, T. Tsuneda, T. Yanai, K. Hirao, *J. Chem. Phys.* **2001**, *115*, 3540.
13. S. Grimme, J. Antony, S. Ehrlich, H. Krieg, *J. Chem. Phys*. **2010**, *132*, 154104.

5 General Conclusion

This dissertation has shown that the theoretical research on the compounds with characteristic bonds which are stimuli-responsive. In Chapter 1, the overview and purpose of this dissertation were described. And then, the targeted compounds and the fundamental concepts about the compounds with characteristic bond were introduced.

In chapter 2, the mechanism of the ligand coupling reaction of the hypervalent pentacoordinate Sb compounds having 3c-4e bond is summarized. It revealed that the ligand coupling reaction caused involving a part of the 3c-4e bond and it clarified the stability due to the electron withdrawing property of the ligand in the transition state.

In chapter 3, I summarize what the organic compound with C–C single bond exceeding 1.7 Å resulted in the C–C single bond due to the cause. The extension of the C–C bond causes due to steric hindrance of the peripheries, and it revealed that underestimation by intramolecular interaction derived from the π skeleton and the existence of molecules in the periphery. In addition, the extension of C–C single bond length with temperature rise was indicated from theoretical calculation.

In chapter 4, I investigated the phenomena caused by the compound having an “ultralong” C–C single bond which I dealt with in Chapter 3 using theoretical calculations. The difference between the symmetry obtained in the crystal structure and the symmetry obtained by NMR analysis was investigated and found that the distortion angle causes "flip" while twisting. In addition, I performed the calculations for cation radical and dication, and I revealed that the cation radical structure is close to that of dication, whose ultralong C–C bond are cleaving.

In the Chapter 1, the stimuli-responsive compounds with the characteristic covalent bond are referred. The change of the physical properties or the chemical reaction which

are related with the characteristic bonds might be a means to make use of new novel materials. I expect that this research is a kind of the standards to pursue the properties of stimuli-responsive compounds.

Acknowledgement

First, I would like to show the greatest gratitude to Prof. Tetsuya Taketsugu, Prof. Masato Kobayashi for highly suggestive advices, discussions, and generous helps. I am also thankful to Prof. Takeshi Iwasa, Prof. Tomoko Akama, Dr. Yuriko Ono, and Dr. Yusuke Kondo for the helpful discussions and advices. I express appreciation to all members of the laboratories I have belonged to during my bachelor, master and doctoral course. I also would like to show my greatest appreciation to Prof. Kin-ya Akiba, professor emeritus of Hiroshima University about the contents in Chapter 2. Moreover, I gratitude Prof. Takanori Suzuki, and Prof. Yusuke Ishigaki about the contents in Chapter 3 and 4. Finally, I would like to appreciate my family members for allowing me to decide to go to doctoral course.